

AD-A040 204

NAVAL POSTGRADUATE SCHOOL MONTEREY CALIF
AN INVESTIGATION OF THE NUCLEAR CONTINUUM IN THE FISSIONABLE NU--ETC(U)
MAR 77 W A HOUK, R W MOORE

F/G 20/8

UNCLASSIFIED

| OF |
AD
A040 204

NL



END

DATE
FILED
6 - 77

(2)
JL

NAVAL POSTGRADUATE SCHOOL

Monterey, California

AD A 040 204



THESIS

AN INVESTIGATION OF THE
NUCLEAR CONTINUUM IN THE
FISSIONABLE NUCLEUS ^{238}U
WITH 87.5 MeV ELECTRONS

by

William Alvah Houk

and

Richard Warren Moore

March 1977

Thesis Advisors:

F. R. Buskirk
R. Pittman

AD No.
DDC FILE COPY

Approved for public release; distribution unlimited.

UNCLASSIFIED

SECURITY CLASSIFICATION OF THIS PAGE (When Data Entered)

REPORT DOCUMENTATION PAGE		READ INSTRUCTIONS BEFORE COMPLETING FORM
1. REPORT NUMBER <i>(6)</i>	2. GOVT ACCESSION NO.	3. RECIPIENT'S CATALOG NUMBER
4. TITLE (and Subtitle) An Investigation of the Nuclear Continuum in the Fissionable Nucleus <i>U-238</i> with 87.5 MeV Electrons. <i>U-238</i>		5. TYPE OF REPORT & PERIOD COVERED Master's Thesis, March 1977
6. AUTHOR(s) William Alvah Houk Richard Warren Moore		7. PERFORMING ORG. REPORT NUMBER
8. CONTRACT OR GRANT NUMBER(S)		9. PERFORMING ORGANIZATION NAME AND ADDRESS Naval Postgraduate School Monterey, California 93940
10. PROGRAM ELEMENT, PROJECT, TASK AREA & WORK UNIT NUMBERS		11. CONTROLLING OFFICE NAME AND ADDRESS Naval Postgraduate School Monterey, California 93940
12. REPORT DATE <i>(11) March 1977</i>		13. NUMBER OF PAGES <i>(12) 61</i>
14. MONITORING AGENCY NAME & ADDRESS (if different from Controlling Office) Naval Postgraduate School Monterey, California 93940		15. SECURITY CLASS. (of this report) Unclassified
16. DISTRIBUTION STATEMENT (of this Report) Approved for public release; distribution unlimited.		15a. DECLASSIFICATION/DOWNGRADING SCHEDULE
17. DISTRIBUTION STATEMENT (of the abstract entered in Block 20, if different from Report)		
18. SUPPLEMENTARY NOTES		
19. KEY WORDS (Continue on reverse side if necessary and identify by block number) Electroexcitation Uranium 238 Giant Resonance <i>U-238</i>		
20. ABSTRACT (Continue on reverse side if necessary and identify by block number) <i>U-238</i> Electroexcitation of <i>U-238</i> between 5 and 40 MeV was accomplished using 87.5 MeV electrons. Data were recorded at scattering angles of 45°, 60°, 75° and 90° and an analysis was made using DWBA calculations and the hydrodynamic model. The results agree with the known positions, widths and cross sections of the Giant Dipole Resonances at $E_x = 10.9$ MeV and 14.0 MeV thus confirming the validity of our evaluation method.		

251450✓82

UNCLASSIFIED

SECURITY CLASSIFICATION OF THIS PAGE(When Data Entered)

In addition, isoscalar and isovector E2 resonances and an isovector E3 resonance were found at 9.9 MeV ($\Gamma = 2.9$), 21.5 MeV ($\Gamma = 4.9$), and 28.4 MeV ($\Gamma = 8.1$), exhausting 39%, 50% and 88% of the respective EWSR. Although isospin cannot be determined from (e, e') , ΔT assignments were based on microscopic and macroscopic considerations.

delta

gamma

ACCESSION FOR	
NTIS	White Section <input checked="" type="checkbox"/>
DOC	Buff Section <input type="checkbox"/>
UNANNOUNCED	<input type="checkbox"/>
JUSTIFICATION	
BY	
DISTRIBUTION/AVAILABILITY CODES	
Dist.	AVAIL. and/or SPEC.
<i>A</i>	

Approved for public release; distribution unlimited

An Investigation of the
Nuclear Continuum in the
Fissionable Nucleus ^{238}U
with 87.5 MeV Electrons

by

William Alvah Houk
Lieutenant, United States Navy
B.S., University of Nebraska, 1970

and

Richard Warren Moore
Lieutenant Commander, United States Navy
B.S., United States Naval Academy, 1967

Submitted in partial fulfillment of the
requirements for the degree of

MASTER OF SCIENCE IN PHYSICS

from the

NAVAL POSTGRADUATE SCHOOL
March 1977

Authors

William Alvah Houk
Richard Warren Moore

Approved by:

Fred R Bushnell Thesis Co-Advisor

Rainer Pitham

Thesis Co-Advisor

John M. Dyer

Second Reader

K. G. Walker

Chairman, Department of Physics and Chemistry

Robert W. Johnson

Dean of Science and Engineering

ABSTRACT

Electroexcitation of ^{238}U between 5 and 40 MeV was accomplished using 87.5 MeV electrons. Data were recorded at scattering angles of 45° , 60° , 75° and 90° and an analysis was made using DWBA calculations and the hydrodynamic model. The results agree with the known positions, widths and cross sections of the Giant Dipole Resonances at $E_x = 10.9$ MeV and 14.0 MeV thus confirming the validity of our evaluation method. In addition, isoscalar and isovector E2 resonances and an isovector E3 resonance were found at 9.9 MeV ($\Gamma = 2.9$), 21.5 MeV ($\Gamma = 4.9$) and 28.4 MeV ($\Gamma = 8.1$), exhausting 39%, 50% and 88% of the respective EWSR. Although isospin cannot be determined from (e, e') , ΔT assignments were based on microscopic and macroscopic considerations.

TABLE OF CONTENTS

I.	INTRODUCTION -----	9
II.	EXPERIMENTAL DETAILS -----	11
III.	THEORY -----	12
	A. GENERAL -----	12
	B. ELECTRON SCATTERING -----	13
	C. NUCLEAR DEFORMATION -----	18
	D. NUCLEAR MODELS -----	20
	E. SUM RULES -----	22
IV.	DATA ACQUISITION/ANALYSIS -----	24
V.	RESULTS -----	28
	A. GENERAL -----	28
	B. THE ISOSCALAR GIANT QUADRUPOLE RESONANCE -----	28
	C. THE ISOVECTOR GIANT DIPOLE RESONANCE -----	29
	D. THE ISOVECTOR GIANT QUADRUPOLE RESONANCE -----	30
	E. THE ISOVECTOR GIANT OCTUPOLE RESONANCE -----	30
	F. OTHER STATES -----	31
VI.	CONCLUSIONS -----	32
	LIST OF REFERENCES -----	58
	INITIAL DISTRIBUTION LIST -----	61

LIST OF TABLES

I.	Experimental Parameters -----	34
II.	Half-Density Radius and Surface Thickness -----	35
III.	Data Analysis Results -----	36
IV.	Giant Resonances -----	38
V.	Comparison of Giant Quadrupole Resonances -----	39
VI.	Comparison of Giant Dipole Resonances -----	40

LIST OF FIGURES

1.	Arbitrarily normalized DWBA cross sections for E1 to E4 transitions calculated with the Goldhaber-Teller model -----	41
2.	DWBA cross section for E1 (long axis) and E1 (short axis) transitions calculated with the Goldhaber-Teller model -----	42
3.	Inelastic ^{238}U spectrum 45° -----	43
4.	Inelastic ^{238}U spectrum 60° -----	44
5.	Inelastic ^{238}U spectrum 75° -----	45
6.	Inelastic ^{238}U spectrum 90° -----	46
7.	Inelastic (e, e') spectrum for 45° , radiation tail and background subtracted -----	47
8.	Inelastic (e, e') spectrum for 60° , radiation tail and background subtracted -----	48
9.	Inelastic (e, e') spectrum for 75° , radiation tail and background subtracted -----	49
10.	Inelastic (e, e') spectrum for 90° , radiation tail and background subtracted -----	50
11.	Inelastic cross section for E2 resonance at 9.88 MeV -----	51
12.	Inelastic cross section for E1 (long axis) resonance at 10.77 MeV -----	52
13.	Inelastic cross section for E1 (short axis) resonance at 13.94 MeV -----	53
14.	Inelastic cross section for E2 resonance at 21.55 MeV -----	54
15.	Inelastic cross section for E3 resonance at 28.40 MeV -----	55

ACKNOWLEDGEMENTS

Professor R. Pitthan was the single most important factor which enabled this thesis to be completed. His extensive knowledge of the theory behind this experiment was a constant source of information in moments of crisis. Throughout the period of data analysis, only the total commitment of his time and effort made the timely completion of this project possible.

We are greatly indebted to Professor F. R. Buskirk for his invaluable instruction in the theoretical aspects of this work, as well as the late hours required of him while the Linear Accelerator was in operation.

Both of these gentlemen suffered the traumas of guiding this team through the maze of obstacles toward a meaningful work. For this we are most grateful.

A special thanks goes to Professor J. N. Dyer for laying the foundations for our interest in this area, the technicians Mr. H. McFarland and Mr. D. Snyder for keeping the LINAC fully operational and the members of the W. R. Church Computer Center staff for their patience and assistance.

Finally, we thank our wives and families for their patience and encouragement during the past year.

I. INTRODUCTION

From the late 1930's until the present, photonuclear reactions have been used to study nuclear structure. Several groups have investigated ^{238}U with this method. These include Bar-noy and Moreh (BarM 74) and Gurevich, et al. (GurL 76) who employed bremsstrahlung beams and Veyssi  re, et al. (VeyB 73) and Caldwell, et al. (CalD 76) who used monochromatic photons. The four above research groups located the maxima of the two Giant Dipole Resonance (GDR) branches in ^{238}U at excitation energies of about 10.9 MeV and 14.0 MeV.

Lewis and Horen (LewH 74) measured ^{238}U (p, p'). A "bump-like" resonance was found in the 10-13 MeV excitation energy range which was interpreted as a quadrupole resonance. Approximately 85% of the isoscalar sum rule was exhausted in this measurement.

Wolynec, Martins and Moscati (WolM 76) have used the ^{238}U ($e, e'\alpha$) ^{234}Th reaction to investigate the Giant Quadrupole Resonance (GQR). Approximately 50% of the isoscalar energy-weighted sum rule (EWSR) was exhausted by a Breit-Wigner shaped resonance at 8.9 MeV with $\Gamma = 3.7$ MeV.

Inelastic electron scattering was not used to identify and locate Giant Resonances in medium and heavy nuclei until about 1970, when both Magnetic Dipole and Electric Quadrupole Giant Resonances were identified in $N = 82$ nuclei (PitW 71). Since that time several (e, e') groups have been investigating

nuclei of interest. This experiment is the first investigation of a fissionable nucleus in the excitation range up to 40 MeV.

II. EXPERIMENTAL DETAILS

^{238}U was the target of 87.5 MeV electrons from the Naval Postgraduate School 120 MeV Linear Accelerator. Data were collected at constant incident electron beam energy and at scattering angles from 45° to 90° in 15° increments, thus using the variation of the momentum transfer with angle to investigate Giant Resonances. A wider spread of angles was not necessary because the maxima of E1 to E4 form factors were included within this range (Figure 1 and 2). The evaluation of backward angles was not a part of this experiment, therefore magnetic transitions were not observed.

Samples of 99.9% enriched ^{238}U were obtained from Ventrion Corp. and Research Organic/Inorganic Corp. and rolled to 0.004 inches for the 90° scattering angle, 0.002 inches for the 75° and 60° scattering angles and 0.001 inches for the 45° scattering angle. Using the three different target thicknesses made it possible to optimize count rate while achieving the required statistical accuracy. A summary of experimental parameters is listed in Table I. The general arrangement of the NPS linear accelerator is described by Pitthan, et al. (PitB 77).

III. THEORY

A. GENERAL

Nuclei exhibit a shell structure in the approximation of independent particle motion. When a nucleus is struck by an outside particle, one of the nucleons is excited into a higher level, leaving a hole in the shell of the nucleus. If there is enough energy in the collision, the target nucleon may be removed from the nucleus altogether. The final states resulting from this excitation are generally particle-unstable and broadened so individual states often cannot be seen. Since the cross section for the photon excitation of these states is large, they were called Giant Dipole Resonances.

In a single particle excitation, the energy of the Giant Quadrupole Resonance (GQR) should be $2\hbar\omega_0$ (i.e., $\Delta n=2$ in the shell model); but the strong collective nature of the resonance implies that many nucleons are excited and find themselves in a distorted potential produced by the now partly empty shells. This lowers the resonance energy by a factor of $\sqrt{2}$ or

$$E_x = \frac{1}{\sqrt{2}} (2\hbar\omega_0) = 58A^{-1/3} \text{ MeV.}$$

In addition to the above isoscalar resonance, experiments show, and theory predicts, an isovector E2 resonance at higher energy, namely $130A^{-1/3}$ MeV (BohM 75).

A similar picture is gradually evolving for the Giant Octupole Resonance, but due to the fact that in this case $1\hbar\omega_0$ and $3\hbar\omega_0$ transitions are allowed by the shell model, the situation is more complex. Generally it appears that those occurring at lower energies are isoscalar ($\Delta T=0$) excitations which correspond to the collective motion of neutrons and protons in phase

with each other. At higher energies the isovector ($\Delta T=1$) states appear because of the out-of-phase movement of neutron and protons (BohM 75).

Another way to explain the same phenomenon is similar to the theory of semiconductors. There is an interaction between the particle and the hole. This particle-hole interaction is attractive for isoscalar and repulsive for isovector states. For E2 excitations it thus raises the latter state to about $130A^{-1/3}$ MeV and lowers the former type of resonance from about $80A^{-1/3}$ MeV expected from the shell model to about $60A^{-1/3}$ MeV as predicted by Bohr and Mottelson (BohM 75).

B. ELECTRON SCATTERING

Electron scattering has distinct advantages over photonuclear reactions and Coulomb excitation by heavy, charged particles. In photonuclear reactions, where the photon is absorbed in the nucleus, the amount of the momentum transfer is proportional to the energy of the photon by

$$E = pc = \hbar\omega.$$

Photon absorption excites predominantly the E1 transitions. Usually only the (γ, n) channel is measured. For a fissionable nucleus, such as ^{238}U , the $(\gamma, \text{fission})$ cross section is large while the (γ, p) cross section is small due to the Coulomb barrier. In this case, the total photonuclear cross section is assumed to be the summation of the (γ, n) and the $(\gamma, \text{fission})$ cross sections. Electron scattering is more informative than the photonuclear reactions partly because all reaction channels are used, and also due to the ability to vary the momentum, q , transferred to the nucleus for a given constant excitation energy, E_x . This allows one to excite multipolarities other

than E_1 . Coulomb excitation by the electric field of incident, heavy charged particles does not noticeably excite magnetic transitions, but these can be excited by (e, e') at backward angles.

For elastic scattering by any nucleus, the magnitude of the momentum transfer is given by

$$q = (k_1^2 + k_2^2 - 2k_1 k_2 \cos \theta)^{\frac{1}{2}},$$

where k_1 and k_2 are the incident and scattered electron momentum respectively and θ is the scattering angle. For incident and scattered electron energies that are much greater than the electron rest mass, the momentum transfer simplifies to

$$q^2 = 4k_1 k_2 \sin^2 \frac{\theta}{2}.$$

By varying the scattering angle, various values of momentum transfer are achieved.

The cross section for elastic electron scattering in the plane wave Born approximation is determined by

$$\left(\frac{d\sigma}{d\Omega}\right)_{OBS} = \left(\frac{d\sigma}{d\Omega}\right)_{MOTT} \left| \int \rho(\vec{r}) e^{i\vec{q} \cdot \vec{r}} d\tau \right|^2,$$

where $\rho(\vec{r})$ is the nuclear charge density as a function of the radius vector from the center of the nucleus and \vec{q} is the momentum transfer vector. The expression under the integral is called the form factor and contains all the information concerning the nuclear structure. The Mott cross section for a relativistic electron, scattered from a nucleus of point charge Ze , neglecting recoil, is

$$\left(\frac{d\sigma}{d\Omega}\right)_{MOTT} = \left(\frac{Ze^2}{2E_i}\right)^2 \frac{\cos^2 \theta/2}{\sin^4 \theta/2},$$

where E_i is the incident electron energy.

Electrons are inelastically scattered if they lose energy due to the excitations of transitions from the ground state of the nucleus to an excited state. The form for the inelastic

scattering cross section has both longitudinal and transverse parameters (IsaB 63) and is far more complicated than that for elastic scattering.

In the plane wave Born approximation, the differential inelastic cross section is the sum over the separate electric and magnetic multipole transition cross sections (The 72),

$$\left(\frac{d\sigma}{d\Omega}\right)_{PWBA} = \sum_{\lambda} \left(\frac{d\sigma}{d\Omega}\right)_{E\lambda} + \sum_{\lambda} \left(\frac{d\sigma}{d\Omega}\right)_{M\lambda},$$

with the electric multipole terms given by

$$\begin{aligned} \left(\frac{d\sigma}{d\Omega}\right)_{E\lambda} &= \alpha^2 a_{\lambda} q^{2\lambda} k_o^{-2} [\lambda(\lambda+1)^{-1} B(C\lambda, q, I_o \rightarrow I_x) V_L(\theta) \\ &\quad + B(E\lambda, q, I_o \rightarrow I_x) V_T(\theta)] R^{-1} \end{aligned}$$

and the magnetic multipole terms by

$$\left(\frac{d\sigma}{d\Omega}\right)_{M\lambda} = \alpha^2 a_{\lambda} q^{2\lambda} k_o^{-2} B(M\lambda, q, I_o \rightarrow I_x) V_T(\theta) R^{-1}.$$

For these equations

$$a_{\lambda} = 4\pi \lambda^{-1} (\lambda+1)[(2\lambda+1)!!]^{-2},$$

$$k_o = E_o / \hbar c,$$

$$R = 1 + \hbar c (k_o/Mc^2)(1 - \cos \theta),$$

where

λ = transition multipolarity,

α = fine structure constant,

E_0 = primary electron energy,

θ = scattering angle,

M = nuclear mass.

R is a factor which accounts for the recoil of the nucleus.

The (four vector) nuclear current density is divided into two components which are parallel, ($v_L(\theta)$), and perpendicular, $v_T(\theta)$, to the momentum transfer (three vector) q:

$$v_L(\theta) = \frac{1}{4} \left(\frac{\cos^2 \theta/2}{\sin^4 \theta/2} \right) ,$$

$$v_T(\theta) = \frac{1}{8} \left(\frac{1+\sin^2 \theta/2}{\sin^4 \theta/2} \right) .$$

$v_L(\theta)$ corresponds to the electron interacting with the nuclear charge and $v_T(\theta)$ involves the nuclear current and magnetization density contributions. The current, charge and magnetization densities are the matrix elements of the respective transition operators between initial and final nuclear states (The 72). These operators in turn are used to obtain the reduced transition probabilities (B-values).

The theoretical form factor can be computed by the Born approximation, which is good for light nuclei, in which the incident and scattered electron wave functions are assumed to be plane waves. As the Z of the nucleus increases, the Coulomb field surrounding the nucleus distorts the incident and scattered electron wave functions requiring the use of the distorted wave Born approximation. The distorted waves are calculated by solving the Dirac equation numerically with a computer program (Tuaw 68).

The experimental cross sections for various values of momentum transfer are compared to the DWBA cross sections calculated with the Goldhaber-Teller model. The multipolarity assignment of the resonance is based on the DWBA curve which best compares with the experimental cross sections.

In the limit as $q \rightarrow k = E_x / \hbar c$ (the so-called photon point), $B(E\lambda, q)$ and $B(M\lambda, q)$ become the reduced matrix elements for γ transitions. Electron scattering mostly uses the B-values at $q = 0$, which are

$$B(E\lambda) = (2\lambda+1) \left[\int r^2 Y_{\lambda M} \rho_{tr}(\vec{r}) d\tau \right]^2,$$

where $Y_{\lambda M}$ is the spherical harmonic function and $\rho_{tr}(\vec{r})$ is the transition charge density (ZieP 68).

The square of the form factor is related to the reduced transition probability $B(E\lambda)$ by

$$B(E\lambda) = \frac{|F(q^2)|^2}{|F(q^2)|^2_{DWBA}} \exp^{-2\lambda},$$

since the DWBA calculations are normalized to $B = 1 e^2 fm^{2\lambda}$.

C. NUCLEAR DEFORMATION

Nuclei have a tendency towards achieving and maintaining closed shells; spherical shape occurs with a closed shell. By adding several nucleons outside the closed shells, the spherical stability is altered and the nucleus becomes a prolate spheroid. Deformation increases until the next shell becomes half-filled, then the spheroids become less prolate until spherical symmetry returns when the next shell is filled. During this process there is a force associated with the Coulomb energy of the charged sphere (closed shell) which resists deformation caused by the outside nucleons. There are also pairing forces between two nucleons which cause coupling of the angular momentum and result in a total angular momentum for the pair equal to zero.

One can imagine the closed shell nucleus as a charged sphere with an impenetrable but deformable surface membrane. As two protons are added outside the closed shell it would be reasonable to assume the two would migrate to opposite sides of the sphere due to the Coulomb repulsion. This would result in a small deformation of the overall spherical configuration. With the pairing force between the nucleons, the two protons couple together with a total angular momentum equal to zero. This coupling is more effective in spherical nuclei than in those that are deformed. At small deformations, the pairing force will strongly tend to restore spherical symmetry; but at large deformations, there is very little effect (Szy 70).

Deformation of nuclei shows up clearly in Giant Resonance research. The Giant Dipole state of the nucleus splits because a nuclear vibration along the short axis has a higher frequency, and one in the direction of the long axis has a lower frequency. Due to the increasing number of sublevels, the splitting is not noticeable for multipole resonances higher than the GDR, but a broadening has been observed (MooB 76). Bohr and Mottelson (BohM 75) state that the GDR splitting is proportional to the deformation of the nucleus by

$$(\bar{E})^{-1} [E(v=1) - E(v=0)] \sim \frac{\Delta R}{R},$$

where $(\bar{E})^{-1}$ is the mean resonance energy and ΔR is the difference between the principal axes of the nucleus. The $v = 0$ term represents oscillations in the direction of the nuclear symmetry axis and $v = 1$ is associated with oscillations in the two perpendicular directions. Danos (Dan 58) gives the relation between the energies, E_a and E_b , of the splitting of the GDR as

$$\frac{E_b}{E_a} = 0.911 \frac{a}{b} + 0.089,$$

where a and b are the lengths of the long and short axes of the deformed spheroid. He also gives the relationship between the reduced transition probabilities (B) of the long and short axis resonances as 1:2. This ratio has been proven to be approximately right in this experiment as well as in past photonuclear work.

D. NUCLEAR MODELS

Goldhaber and Teller (Golt 48), who gave a theoretical description of the GDR (see also Mig 44), discuss three alternative models for the Giant Dipole Resonance:

1. The force which displaces a proton from its average position in the nucleus is proportional to the displacement. This force will be the same for all nuclei and for every proton in the nucleus. In this model, the GDR has the same excitation energy in every nucleus.

2. Motion of neutrons and protons in the nucleus causes a change in density of the neutron and proton fluids with a restoring force proportional to the gradient of these densities. The excitation energy ($E_x = \hbar\omega$) of the GDR, which varies as the square root of the restoring force, is proportional to $A^{-1/3}$.

3. The neutrons and protons are assumed to behave as two interpenetrating fluids with a restoring force proportional to the surface area. The excitation energy is proportional to the square root of the force, or $A^{-1/6}$.

The second model was expanded in greater detail by Steinwedel and Jensen (SteJ 50) which led to the formula

$$\omega_{qr} \sim 80A^{-1/3} \quad (\text{Ube } 71)$$

In model three, Goldhaber and Teller assume a charge density $\rho_0(r)$ of the ground state was rigidly displaced and the total charge density could be expressed as

$$\rho(r) = \rho_0(r) - \frac{1}{2} \vec{d} \cdot \vec{\nabla} \rho_0(r)$$

if the displacement vector, \vec{d} , between the centers of the neutron and protons spheres were small. The transition charge density $\rho_{tr}(r)$ then is

$$\rho_{tr}(r) = C_{GT} r^{\lambda-1} \left[\frac{d \rho_o(r)}{dr} \right].$$

Überall (Ube 71), in his generalization of the hydrodynamic model, assumes the nucleus to consist of four interpenetrating fluids, neutrons with spin up (n^\uparrow), neutrons with spin down (n^\downarrow), and likewise with protons (p^\uparrow), (p^\downarrow). Oscillation of any two of these fluids 180° in or out of phase against the other two gives rise to four possible collective modes.

1. $(p^\uparrow, p^\downarrow)$ against $(n^\uparrow, n^\downarrow)$, the isospin or Goldhaber-Teller mode (i).
2. (p^\uparrow, n^\uparrow) against $(p^\downarrow, n^\downarrow)$, the spin-wave mode (s).
3. $(p^\uparrow, n^\downarrow)$ against $(p^\downarrow, n^\uparrow)$, the spin-isospin mode (si).
4. All four fluids oscillating in phase. This produces a compressional oscillation called a breathing mode. In this experiment, only the Goldhaber-Teller model was considered for the E1 transitions.

The elastic scattering cross sections were computed with a phase shift program (FisR 64) assuming a Fermi charge distribution

$$\rho(r) = \rho_o [1 + \exp \frac{r-c}{t/4.4}]^{-1},$$

where ρ_o is a normalization density, c is the half density radius, t is the skin or surface thickness and r is the

nuclear radial coordinate. The half density radius is the distance from the center of the nucleus to the point where the density has been reduced to one-half maximum value. The skin thickness is measured between the 10% and 90% points of charge distribution. The values $c = 6.805 \text{ fm}$ and $t = 2.66 \text{ fm}$ were taken from the compilation of DeJager, DeVries and DeVries (DeJD 74). The parameterization into c_{tr} and t_{tr} of Ziegler and Peterson (ZieP 68) was used for the inelastic calculations. Table 2 is the summary of all c_{tr} and t_{tr} values used for the inelastic transition densities in this work. Values of c_{tr}/c different from 1.0 were used for the GDR corresponding to the long and short axes of the deformed uranium nucleus, which were calculated using Danos' formula (Dan 58). The deformed nucleus is treated as two spheres with radii equal to that of the short (a) and long (b) axes of the ellipsoid. The so-called equivalent radius, r_{eq} , is defined as the radius of the sphere which has the same volume as this ellipsoid. The c_{tr} were calculated by multiplying the ground state charge density parameter c with the ratio of a/r_{eq} and b/r_{eq} , respectively; t_{tr} was assumed not to differ from t .

E. SUM RULES

For any quantum mechanical system the energy-weighted sum rule

$$\sum_N | \langle \psi_0 | Q | \psi_N \rangle |^2 (E_N - E_0) = \frac{1}{2} \langle \psi_0 | Q, i\hbar \frac{\partial Q}{\partial t} | \psi_0 \rangle \quad (\text{Irv 72})$$

is valid for any Hermetian operator Q. For (e, e') , the energy-weighted sum rule is especially useful because it depends mainly on the known nuclear charge distribution in the ground state and is insensitive to nucleonic correlations which are strongly model dependent (NatN 66). From this basic definition, various sum rules have been used for electric and magnetic multipole resonance analysis.

In this work the isoscalar sum rule for $\lambda > 1$,

$$S(E\lambda, \Delta T = 0) = \frac{Z^2 e^2 \lambda(\lambda+1)^2 \hbar^2}{8\pi A M_p} \langle R^{2\lambda-2} \rangle, \quad (\text{NatN } 66)$$

was used, where M_p is the mass of the proton and $\langle R^{2\lambda-2} \rangle$ the moment ground state charge distribution of the nucleus. This sum rule does not consider interference terms between isoscalar and isovector excitations. For the isovector resonances of $\lambda > 1$, the sum rule is

$$S(E\lambda, \Delta T = 1) = S(E\lambda, \Delta T = 0) \left(\frac{N}{Z} \right).$$

The energy-weighted isovector sum rule for electric dipole resonances is

$$S(E) = \frac{9e^2 \hbar^2}{8\pi M_p} \left(\frac{NZ}{A} \right) \quad (\text{WarW } 69)$$

Table IV gives the energy-weighted sum rules for ^{238}U calculated with $\langle R^2 \rangle^{\frac{1}{2}} = 5.730 \text{ fm}$ and $\langle R^4 \rangle^{\frac{1}{4}} = 6.124 \text{ fm}$, which in turn were calculated by numerical integration of the ground state charge distribution.

IV. DATA ACQUISITION/ANALYSIS

87.5 MeV electrons were scattered at 45° to 90° scattering angles by self-supporting ^{238}U foils using the NPS 120 MeV LINAC. The targets were positioned to bisect the scattering angle so that the path length of the electrons in the target was at a minimum. The transmission mode was used in order that all the electrons traveled the same path length to reduce line broadening or energy straggling due to ionization. After scattering, the electrons were analyzed in a 16" magnetic spectrometer with a counting system consisting of 10 scintillation counters linearly arranged in the focal plane to cover a 3% momentum range. Table II summarizes basic target and counting system parameters for each run. Data were read from the counting system through an Altair 8800 microcomputer onto a magnetic tape compatible with the IBM 360/67 Computer.

The spectrometer energy was decremented in 0.1 MeV steps. The summation of data from all counters resulted in an elastic and an inelastic scattering spectrum. The latter was analyzed from 5 to 40 MeV excitation energy with a least squares fit program using Breit-Wigner type resonances.

Incorporated into this analysis is the evaluation of the background included in the inelastic spectrum. A large part of this background is the elastic radiation tail which is caused by photon emission before, during and after the scattering event, plus energy straggling and ionization. In this

experiment, the radiation tail was calculated using the formulation, in the Born approximation, of Ginsberg and Pratt (GinP 64), and substituting the actual elastic cross section, based on the phase shift calculation of Fischer and Rawitscher (FisR 64). Along with the radiation tail, general room background, measured with the "target out," and electrons scattered by the target and subsequently scattered by the spectrometer walls, form the total background of the inelastic spectra.

The total background was described as a function of the energy (E_f) of the outgoing electron. Two different background functions were used:

$$BGR(E_p) = P_1 + P_2(1/E_f) + P_3 \cdot RT$$

and

$$BGR(E_f) = P_1 + P_2(E_f - E') + P_3 \cdot RT,$$

where the P_i are the fitting parameters, E' is the energy center of the fitting range and RT is the radiation tail. There was virtually no difference between the results obtained using the two functions. The second function was used in the final analysis of all spectra.

There are three alternate criteria for placement of a resonance in the spectrum; (1) the observation of the resonance peaking above the flat expanse of the radiation tail and background, (2) the knowledge of resonances found by photonuclear and photofission experiments (BarM 74, GurL 76, VeyB 73, WolM 76), (3) the necessity to add a resonance to achieve a consistent overall fit. In the case of uranium, it is difficult to use the first criterion above for reasonable

placement. With electron scattering by heavy nuclei, very few of the collective states are visible to the naked eye in the spectrum, uncorrected for background radiation. It is only after the subtraction of the elastic peak radiation tail and other radiation due to Bremsstrahlung that the spectrum begins to exhibit the structure of the Giant Multipole Resonances. All lines were fitted using the Breit-Wigner line form. This line form was used instead of the Lorentz or Gaussian line forms because it was found to better fit photo-nuclear data by Gordon (Gor 75).

A very large structure was first observed at 45° at the excitation energy of 6.2 MeV with a full width half maximum (Γ) of 4.5 MeV. So unusual was this position and strength that the other angles, as well as older data from both spherical and deformed nuclei, were investigated and a special run was done with ^{12}C . Through analysis of these results, it was determined that the spectrometer itself was causing a pseudo-resonance (ghost peak). The elastically scattered electrons hit the spectrometer wall at a magnetic field of 92% of that corresponding to the elastic line, enhancing the coincidence count rate. The exact position, width and approximate line shape were determined from the well known ^{12}C spectrum. Although the line shape appears to be complex, a Breit-Wigner shape fits closely. The area was a constant fraction of the elastic peak (~.015). This was large enough to envelop any possible collective states from 3.5 MeV to

8.5 MeV excitation energy and made it difficult to evaluate the lower end of the spectrum.

The analysis of the data followed a basic procedure which started with the aforementioned reasons in attempting to fit a resonance at a specific energy. A least squares curve fitting program was used to evaluate the spectra numerically. A value of χ^2 (per degree of freedom) of less than 1.0 (expected value) indicated compatibility of background and the resonance energy, strength and width with the data. Initially, photonuclear results for the GDR were inserted and kept constant. By physically sighting bumps in the spectrum and with the knowledge of the smooth variation of Giant Resonances with mass number from previous work (PitB 74), other lines were inserted into the spectrum.

Once a line was inserted, excitation energy and full width half maximum were held constant to reasonably expected values and the curve fitting program gave the resulting transition strength (B) and χ^2 value. Continuous recycling of the data, using various combinations of resonances, excitation energies and values for full width half maximum, yielded χ^2 values and transition strengths. The overall results of this data analysis for each scattering angle are contained in Table III.

The cross section of each of these resonances was plotted versus momentum transfer and compared to the curves calculated for the DWBA program (TuaW 68). The result was a designation of the multipolarity of the resonance, as well as the strength and half width.

V. RESULTS

A. GENERAL

The results of the curve fitting for each spectrum are given in Table III. In Table IV, the various strengths observed for each line are averaged. As mentioned earlier, Breit-Wigner line shapes were used for all resonances.

Figures 3 through 6 show the inelastic spectrum for all angles at which data were taken. They are corrected for the constant dispersion of the magnetic spectrometer. From these curves several features are noteworthy: (1) the spectrum itself has very little noticeable structure; (2) radiation tail and background are large and present some problem in resonance evaluation; (3) the radiation tail decreases when going from forward to backward angles. However, after subtraction of background (Figures 7 to 10), the variation of resonance strength as momentum transfer increases from 45° to 90° scattering angle can be seen.

Errors in cross section as shown in Figures 11 through 15 were based on the statistical errors. The errors of excitation energy, width and B-values are best estimates from the minimum and maximum values of the parameters which would fit the spectrum, while still achieving a χ^2 of less than 1.1.

B. THE ISOSCALAR GIANT QUADRUPOLE RESONANCE

Figure 11 shows that the resonance found at 9.88 ± 0.21 MeV with a width of $2.88^{+0.77}_{-0.38}$ MeV conforms to an E2 DWBA

cross section. Exhausting 39% of the energy-weighted sum rule, it has a reduced transition probability of 3670 ± 400 fm⁴. Excitation, width and strength (Table V) are in agreement with the (e,e', α) measurements (WolM 76). It is not in agreement with the excitation energy and strength from (p,p') experiments (LewH 74). It certainly is possible that the existence of the ghost resonance in this work could have affected the position and width of this line, which has the lowest excitation energy of those evaluated.

C. THE ISOVECTOR GIANT DIPOLE RESONANCE

As explained above, the GDR ($\Delta T = 1$) is split into two distinct resonances due to the deformation of the nucleus. These two resonances were evaluated with the GT model using two different transition charge distributions with radii proportional to that of the long and short axes of the deformed nucleus.

The GDR associated with the long axis of the nucleus was found to be at 10.77 ± 0.25 MeV with $\Gamma = 3.2 \pm 0.4$ MeV. As seen in Table VI, this is a slightly lower energy than found in either the (γ ,n) results (VeyB 73, CalD 76, GurL 76) or the (γ,γ') experiment (BarM 74). The results of the past and present work agree within the errors. The curve shown in Figure 12 was normalized to the photonuclear (GurL 76) reduced transition probability of 30.4 fm² to show how well the results compare with the known photonuclear information.

Associated with the short axis' of the nucleus is the GDR found at 13.94 ± 0.24 MeV with $\Gamma = 4.45^{+0.22}_{-0.33}$ MeV. Table VI contains the resumé of all work done with this resonance. Figure 13, like Figure 12, is normalized to the photonuclear transition probability of Gurevich, et. al., (40.9 fm^2) (GurL 67). This agreement shows that the evaluation method used is basically correct. The slightly lower excitation energy may be due to the different dependence of the resonance from the excitation energy in (γ, n) and (e, e') (Gor 75).

D. THE ISOVECTOR GIANT QUADRUPOLE RESONANCE

Although some work has been done on the isoscalar GQR region in ^{238}U , there has not been any investigation in the 20 - 40 MeV region. The experiments show an excitation energy of 21.55 ± 0.60 MeV which agrees with the $130A^{-1/3}$ MeV rule found in both spherical (PitB 74) and deformed (MooB 76) nuclei. The width of 4.95 ± 0.55 MeV, but not the strength, $50 \pm 8\%$ EWSR (Table IV), are expected from the trend of the results in ^{208}Pb (PitB 74) and ^{165}Ho (MooB 76). This resonance was not seen in the 45° spectrum however the GQR should be very small at 45° . This negative result is probably due to the ghost peak. The line and arrow drawn in Figure 14 indicate the maximum cross section of the GQR that the curve fitting program would accept, maintaining $\chi^2 \leq 1.0$.

E. THE ISOVECTOR GIANT OCTUPOLE RESONANCE

The E3 strength is more widely distributed and more difficult to locate than the quadrupole strength since the shell

model allows both $1\hbar\omega_0$ and $3\hbar\omega_0$ transitions for octupole excitations, but only $2\hbar\omega_0$ for quadrupole excitations. A resonance comparing favorably with an E3 DWBA cross section (Figure 15) was found at 28.4 ± 1.20 MeV with $\Gamma = 8.07 \pm 1.1$ MeV and exhausting $88 \pm 15\%$ of the EWSR. This excitation energy corresponds to $176A^{-1/3}$ MeV; thus, it is lower than the $195A^{-1/3}$ MeV found in spherical heavy nuclei, but in qualitative agreement with the corresponding resonance in ^{165}Ho . Based on its excitation energy, strength and angular distribution (see discussion in Part III A, above), this resonance should be classified as the $3\hbar\omega$ ($\Delta T=1$) resonance.

F. OTHER STATES

The 45° and 90° spectra (Figures 7 and 10) of this report show one other state which has not been identified or discussed so far. At 17.0 ± 1.8 MeV, a structure of 3.9 ± 1.8 MeV wide is indicated. Although the energy position of $106A^{-1/3}$ MeV closely compares to the isoscalar E3 resonance predicted by the shell model (Ham 72), it does not follow the angular distribution for an E3 cross section. Further investigation is needed to state the multipolarity and strength of this structure.

VI. CONCLUSIONS

The excitation energy range between 5 and 40 MeV was measured in ^{238}U and analyzed for Giant Resonance structure in the continuum. The data are in principal agreement with current experiments and microscopic and macroscopic theoretical considerations. Table IV is a compilation of the results of this experiment.

The following results should be emphasized:

1. In $\text{A}^{-1/3}$ units, the isovector E3 resonance at 28.4 ($176\text{A}^{-1/3}$) MeV has significantly lower excitation energy in ^{238}U than in previously reported spherical nuclei. In ^{197}Au and ^{208}Pb , the resonance was found at 33.5 MeV and 33 MeV respectively (PitB 74), following an $195\text{A}^{-1/3}$ MeV rule. Moore, et. al., (MooB 76) reported the isovector E3 resonance at 34 MeV in ^{165}Ho which would correspond to $186\text{A}^{-1/3}$ MeV. As both ^{238}U and ^{165}Ho are deformed nuclei, it must be concluded that the deformation lowers the expected excitation energy of the shell model.

2. The isoscalar E2 resonance has a lower excitation energy than previously reported in ^{238}U . In addition, only 39% of the isoscalar EWSR is exhausted.

3. Both parts of the isovector GDR, split due to deformation, conform to the photonuclear data.

4. The isovector GQR is in agreement with the $130\text{A}^{-1/3}$ MeV rule found from other nuclei. This resonance was seen in all but the 45° spectrum; but even in the latter case

the analysis would accept a line at the right energy, thus giving an upper limit to the strength.

Future effort should be made in the energy region above 16 MeV to determine the nature of the structure at 17.0 MeV. Furthermore, at low energies, the ghost peak of the Naval Postgraduate School Linear Accelerator dominated the spectrum such that little evaluation was possible below 8.5 MeV. Any improvement which would reduce the ghost peak would aid future measurements.

TABLE I. EXPERIMENTAL PARAMETERS

Spectrometer Angle (Degrees)	Target Thickness (mg/cm ²)	Spectrometer Energy Range (MeV) Elastic	Spectrometer Energy Range (MeV) Inelastic
45	48.13	90.0 - 82.0	85.9 - 45.0
60	91.45	90.0 - 82.0	86.0 - 45.0
75	91.45	90.0 - 82.0	82.0 - 45.0
90	192.64	90.0 - 82.0	82.0 - 45.0

Capacitor Scale (μf)		Integrator Range Scale (Volts)		Beam Current (Amperes)	
Elastic	Inelastic	Elastic	Inelastic	Elastic	Inelastic
0.10	0.10	0.03	10.0	1.4×10^{-9}	1.4×10^{-7}
0.50	0.50	0.30	3.0	5.4×10^{-9}	2.1×10^{-7}
0.50	0.50	0.30	10.0	2.1×10^{-8}	7.1×10^{-7}
0.10	0.10	0.30	10.0	5.4×10^{-8}	8.9×10^{-7}

Elastic Momentum Transfer Squared q^2 (fm ⁻²)	Incident Beam Energy (MeV)
0.116	87.76
0.198	87.74
0.293	87.60
0.387	86.64

TABLE II. HALF DENSITY RADIUS AND SURFACE THICKNESS

Transition	c	t	c _{tr}	t _{tr}
E1 (long axis)	6.805	2.66	1.24	1.00
E1 (short axis)	6.805	2.66	0.90	1.00
E2	6.805	2.66	1.00	1.00
E3	6.805	2.66	1.00	1.00
E4	6.805	2.66	1.00	1.00

TABLE III. DATA ANALYSIS RESULTS

45 DEGREES

Energy (MeV)	Q (fm ⁻¹)	Multipo- larity (E λ)	Form Factor Squared	B Value (fm ^{2λ})
9.77	0.325	E2	1.43X10 ⁻⁴	3.19X10 ³
10.72	0.327	E1	1.34X10 ⁻⁴	2.39X10 ¹
13.80	0.320	E1	4.22X10 ⁻⁴	5.27X10 ¹
17.10	0.318	--	7.76X10 ⁻⁵	-----
21.80	0.315	E2	1.29X10 ⁻⁴	3.00X10 ³
28.50	0.314	E3	4.06X10 ⁻⁵	2.94X10 ⁵

60 DEGREES

Energy (MeV)	Q (fm ⁻¹)	Multipo- larity (E λ)	Form Factor Squared	B Value (fm ^{2λ})
9.87	0.422	E2	2.26X10 ⁻⁴	4.44X10 ³
10.72	0.420	E1	1.09X10 ⁻⁴	2.99X10 ¹
13.98	0.414	E1	3.49X10 ⁻⁴	4.31X10 ¹
21.35	0.402	E2	1.83X10 ⁻⁴	3.49X10 ³
28.55	0.393	E3	2.47X10 ⁻⁴	7.96X10 ⁵

75 DEGREES

Energy (MeV)	Q (fm ⁻¹)	Multipo- larity (E λ)	Form Factor Squared	B Value (fm ^{2λ})
9.87	0.512	E2	1.21X10 ⁻⁴	3.79X10 ³
10.72	0.510	E1	8.50X10 ⁻⁵	2.74X10 ¹
14.08	0.501	E1	1.94X10 ⁻⁴	4.42X10 ¹
21.43	0.483	E2	1.43X10 ⁻⁴	3.58X10 ³
28.40	0.468	E3	1.55X10 ⁻⁴	3.53X10 ⁵

TABLE III. (CONTINUED)

90 DEGREES

Energy (MeV)	Q (fm ⁻¹)	Multipo- larity (Eλ)	Form Factor Squared	B Value (fm ^{2λ})
10.02	0.587	E2	5.39X10 ⁻⁵	3.27X10 ³
10.92	0.584	E1	7.64X10 ⁻⁵	3.12X10 ¹
13.90	0.575	E1	1.75X10 ⁻⁴	5.66X10 ¹
17.10	0.564	--	5.36X10 ⁻⁵	-----
21.63	0.550	E2	1.07X10 ⁻⁴	4.73X10 ³
28.16	0.531	E3	2.38X10 ⁻⁴	5.42X10 ⁵

TABLE IV. GIANT RESONANCES

E_x (MeV)	$E\Delta$	ΔT	$E_x (A^{-1/3})$	$T(\text{MeV})$	B_{calc} ($\text{fm}^2\lambda$)	Strength (SPU)	% EWSR Dissipated
9.88 \pm 0.21	E2	0	62	2.88 \pm 0.77 - 0.38	3.67 $\times 10^3$	17.4	39 \pm 11
10.77 \pm 0.25	E1 (long)	1	67	3.20 \pm 0.40	3.04 $\times 10^1$	5.3	36 \pm 4
13.94 \pm 0.24	E1 (short)	1	86	4.45 \pm 0.22 - 0.33	4.90 $\times 10^1$	9.8	83 \pm 8
21.55 \pm 0.60	E2	1	133	4.95 \pm 0.55	3.61 $\times 10^3$	17.1	50 \pm 8
28.40 \pm 1.20	E3	1	176	8.09 \pm 1.10	6.15 $\times 10^5$	78.0	88 \pm 15

Note: Errors on E_x and T were estimated from the maximum and minimum values that would reasonably fit into the spectrum while still achieving a $\chi^2 < 1.1$.

TABLE V. COMPARISON OF GIANT QUADRUPOLE RESONANCES

Reference	E_x (MeV)	Γ (MeV)	% EWSR	Type of Reaction
LewH 74	10 - 13	-----	85	(p,p')
WolM 76	8.9 ± 0.3	3.7 ± 1.2	50	(e,e', α)
This work	9.88 ± 0.21	2.88 ± 0.77 $- 0.38$	39	(e,e')

TABLE VI. COMPARISON OF GIANT DIPOLE RESONANCES

Reference	Reaction	E_x	Long Axis $\Gamma(\text{MeV})$	B	E_x	Short Axis $\Gamma(\text{MeV})$	B
VeyB 73	(γ, n)	10.96 ± 0.09	2.90 ± 0.14	31.1	14.04 ± 0.13	4.53 ± 0.13	46.5
BarM 74	(γ, γ')	10.95 ± 0.06	2.62 ± 0.19	28.0	14.00 ± 0.68	4.53 ± 0.20	48.3
CalD 76	(γ, n)	10.80	2.44	28.2	13.85	5.12	65.5
GurL 76	(γ, n)	10.97 ± 0.13	2.99 ± 0.48	30.4	14.25 ± 0.18	5.10 ± 0.63	49.0
This work	(e, e')	10.77 ± 0.25	3.20 ± 0.40	28.1	13.94 ± 0.24	4.45 ± 0.22	$49.2 - 0.33$

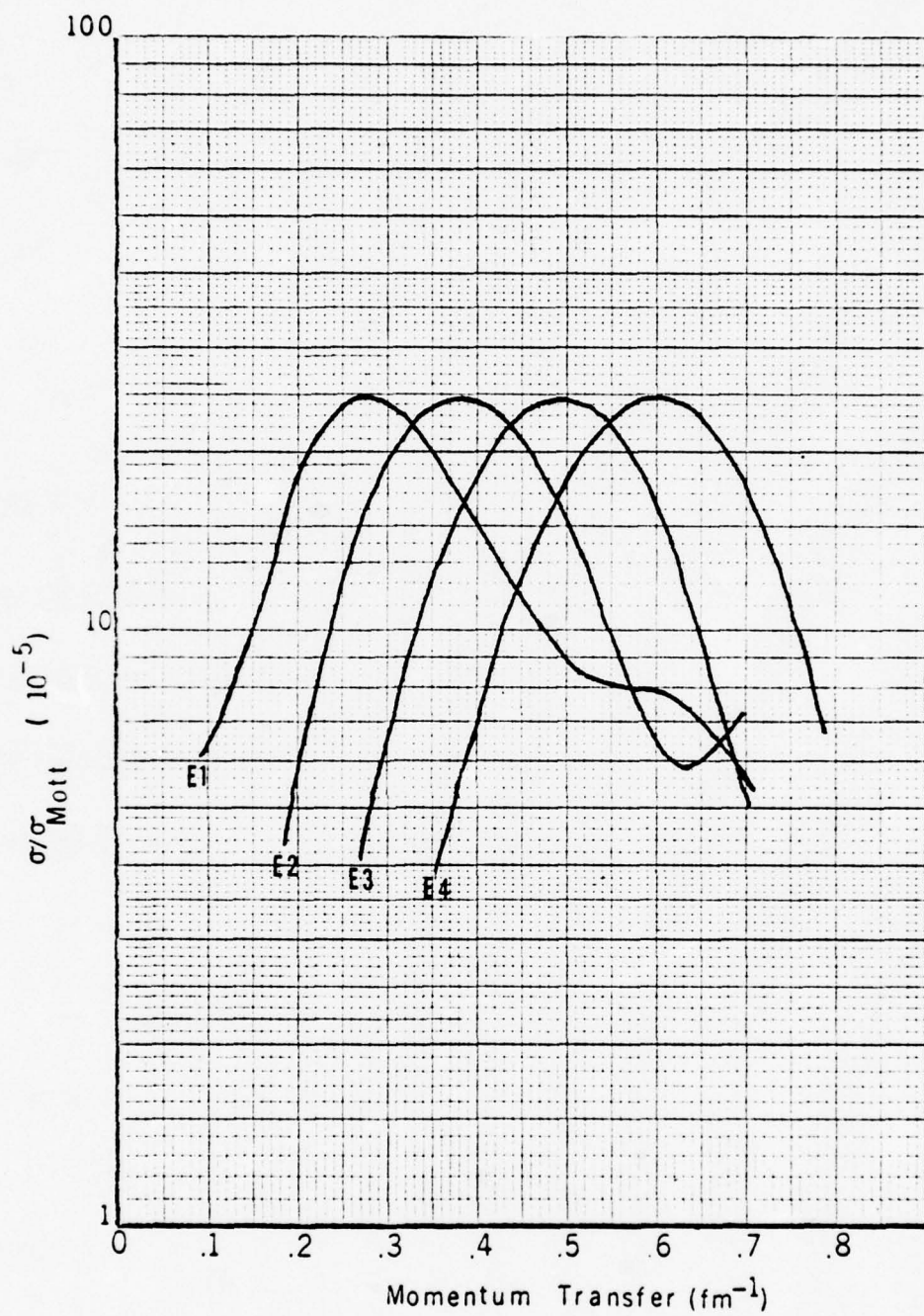


FIGURE 1.

Arbitrarily normalized DWBA cross sections for E1 to E4 transitions calculated with the Goldhaber-Teller model.

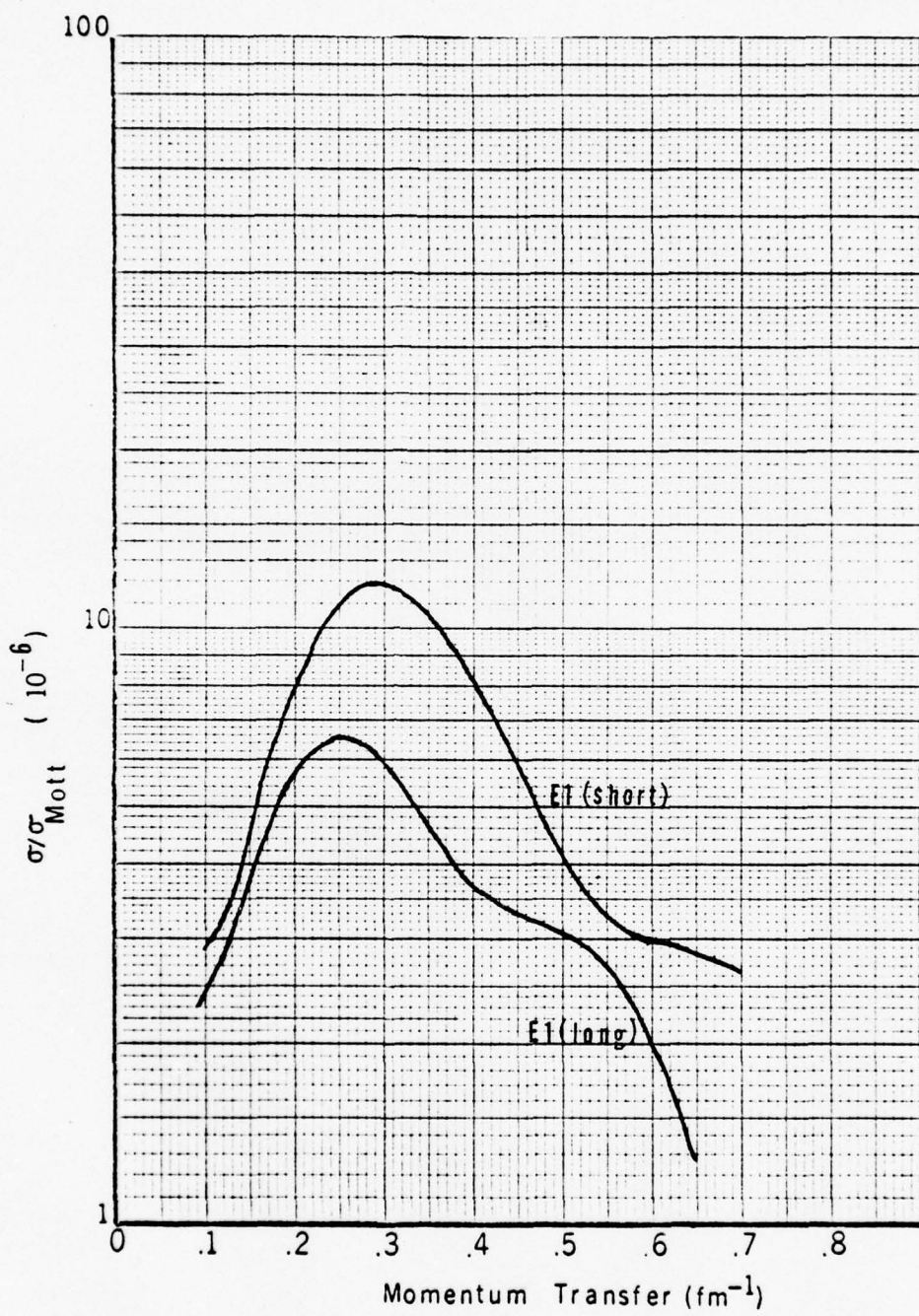


FIGURE 2.

DWBA cross section for E1 (long axis) and E1 (short axis) transitions calculated with the Goldhaber-Teller model.

FIGURE 3.

Inelastic ^{238}U spectrum 45°

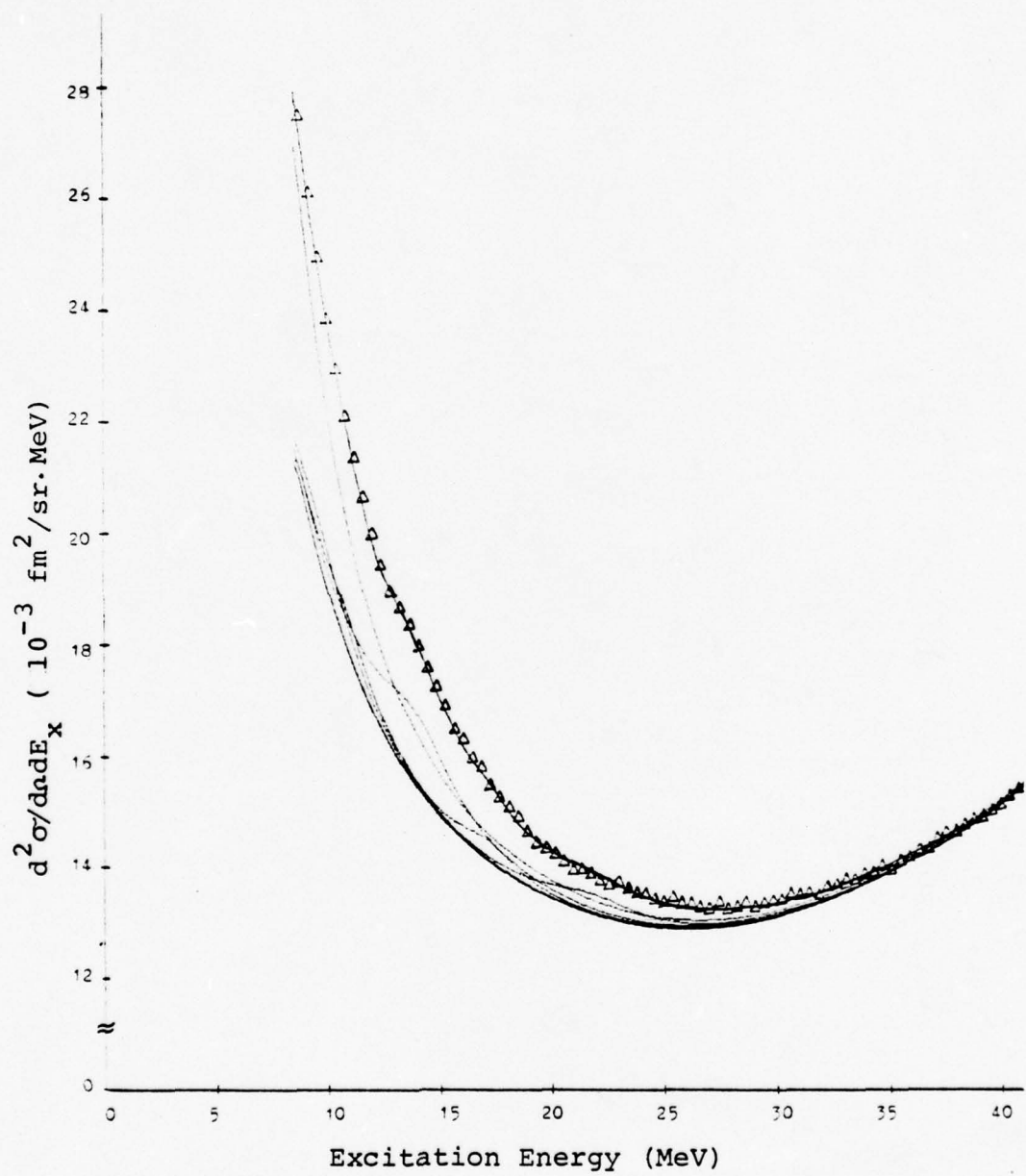


FIGURE 4.

Inelastic ^{238}U spectrum 60°

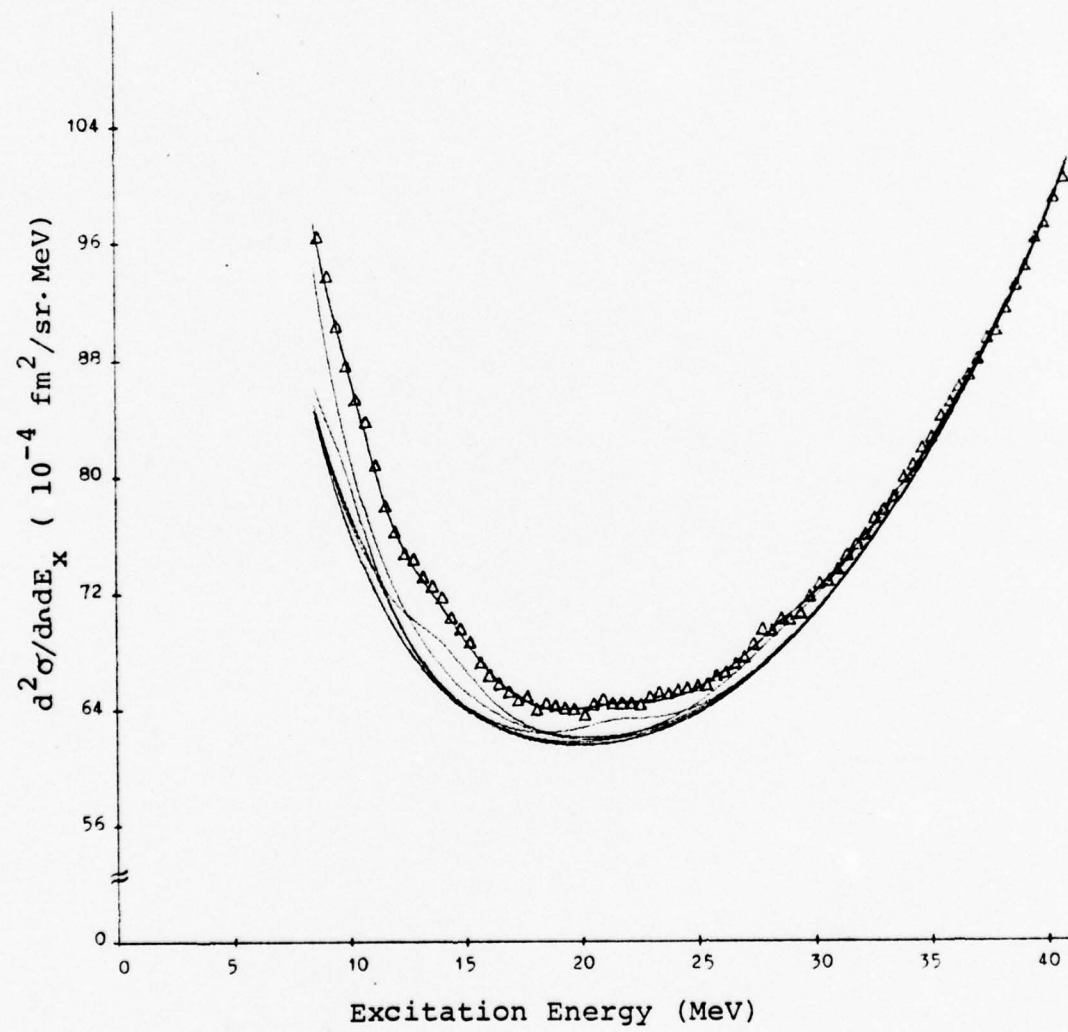


FIGURE 5.

Inelastic ^{238}U spectrum 75°

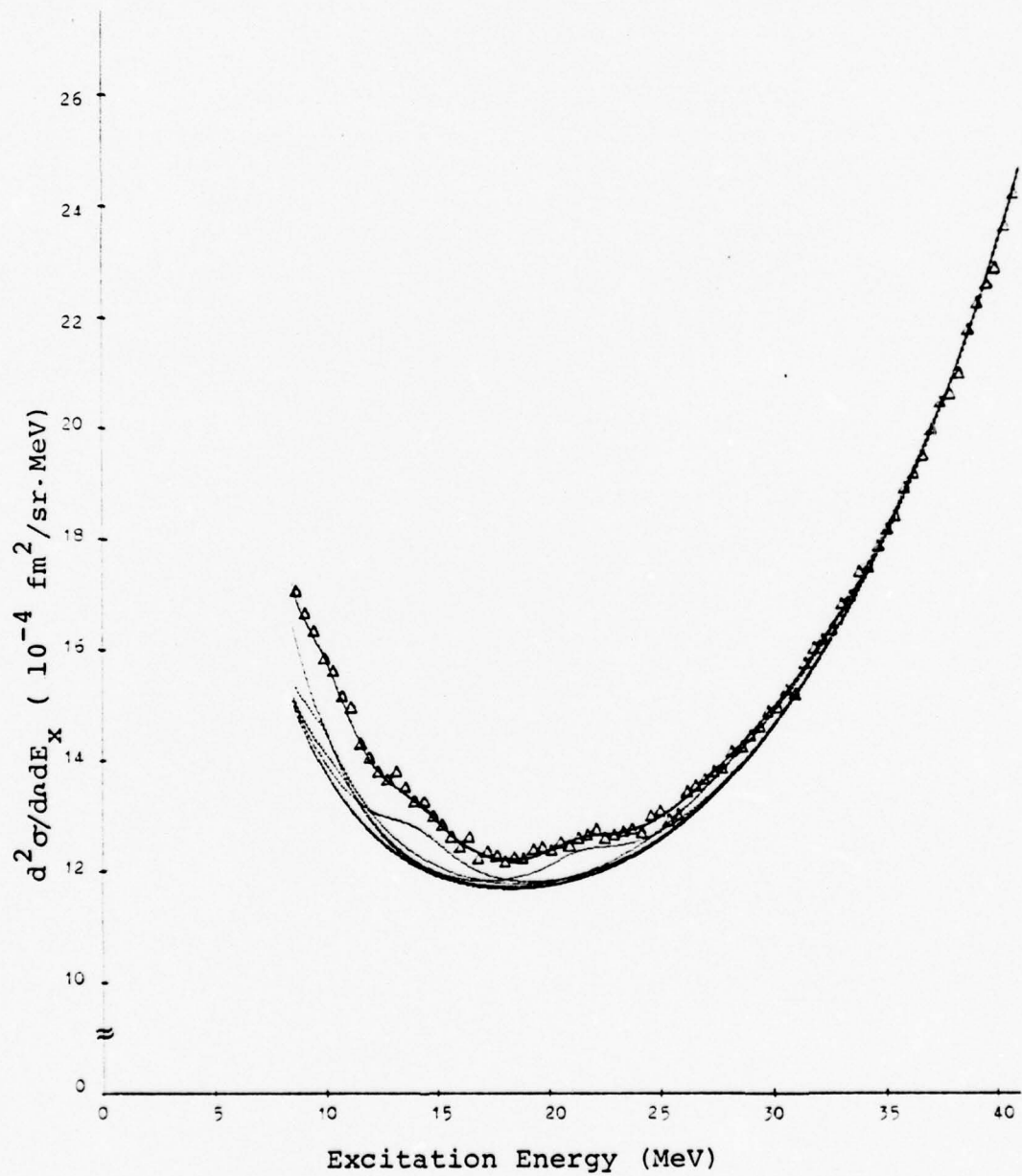


FIGURE 6.

Inelastic ^{238}U spectrum 90°

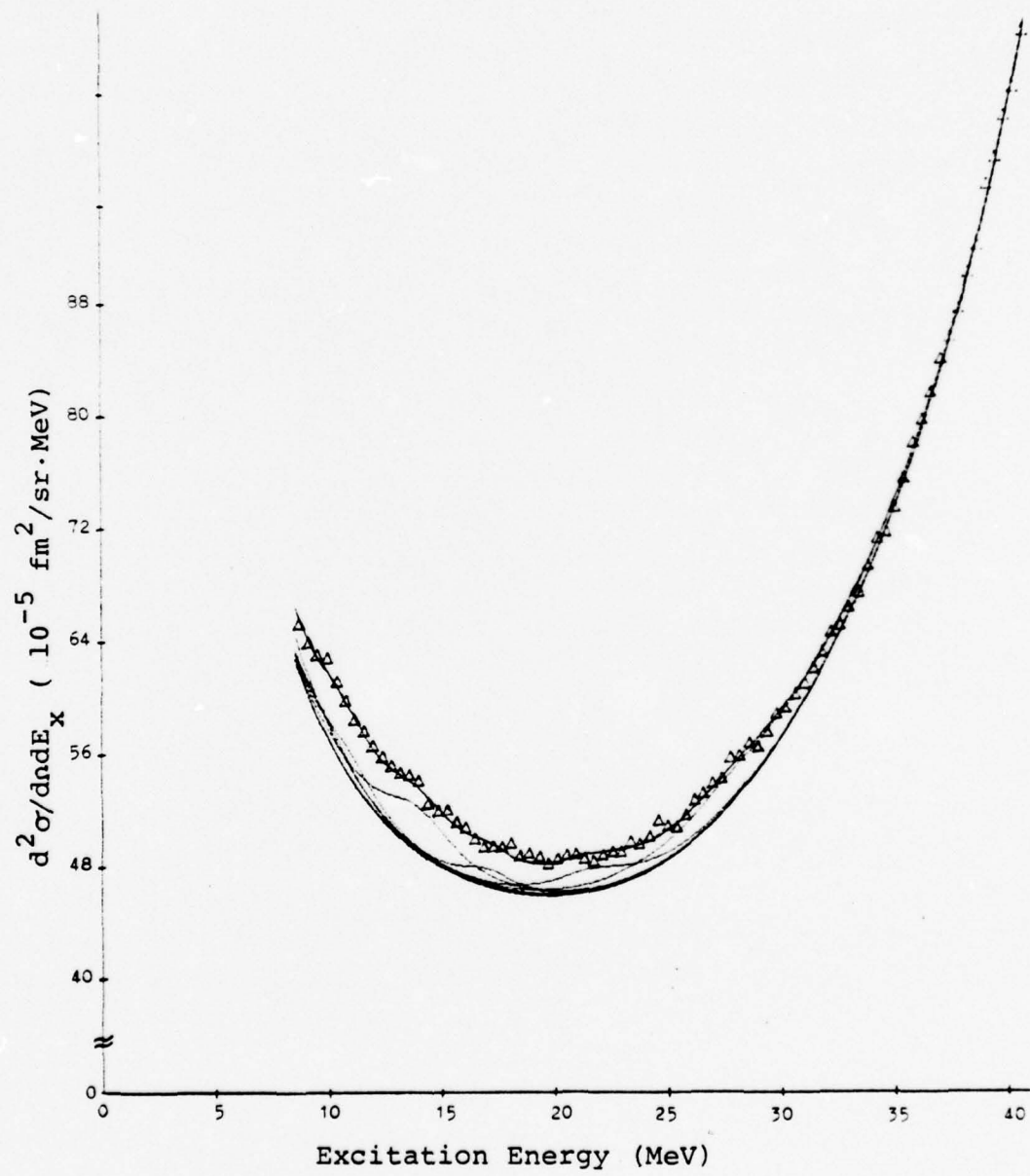


FIGURE 7.

Inelastic (e, e') spectrum for 45° ,
radiation tail and background subtracted.

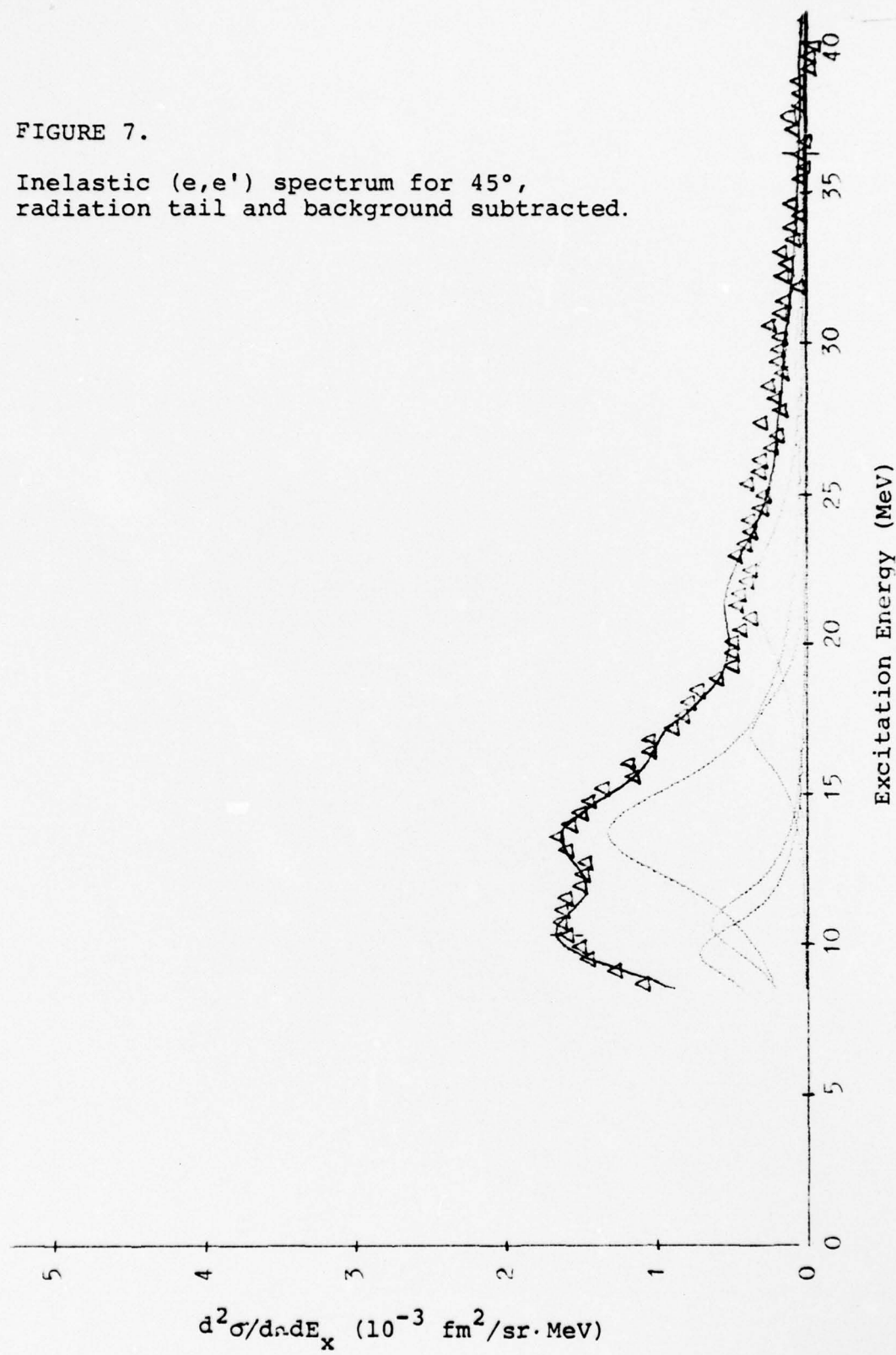


FIGURE 8.

Inelastic (e, e') spectrum for 60° ,
radiation tail and background subtracted.



FIGURE 9.

Inelastic (e, e') spectrum for 75° ,
radiation tail and background subtracted.

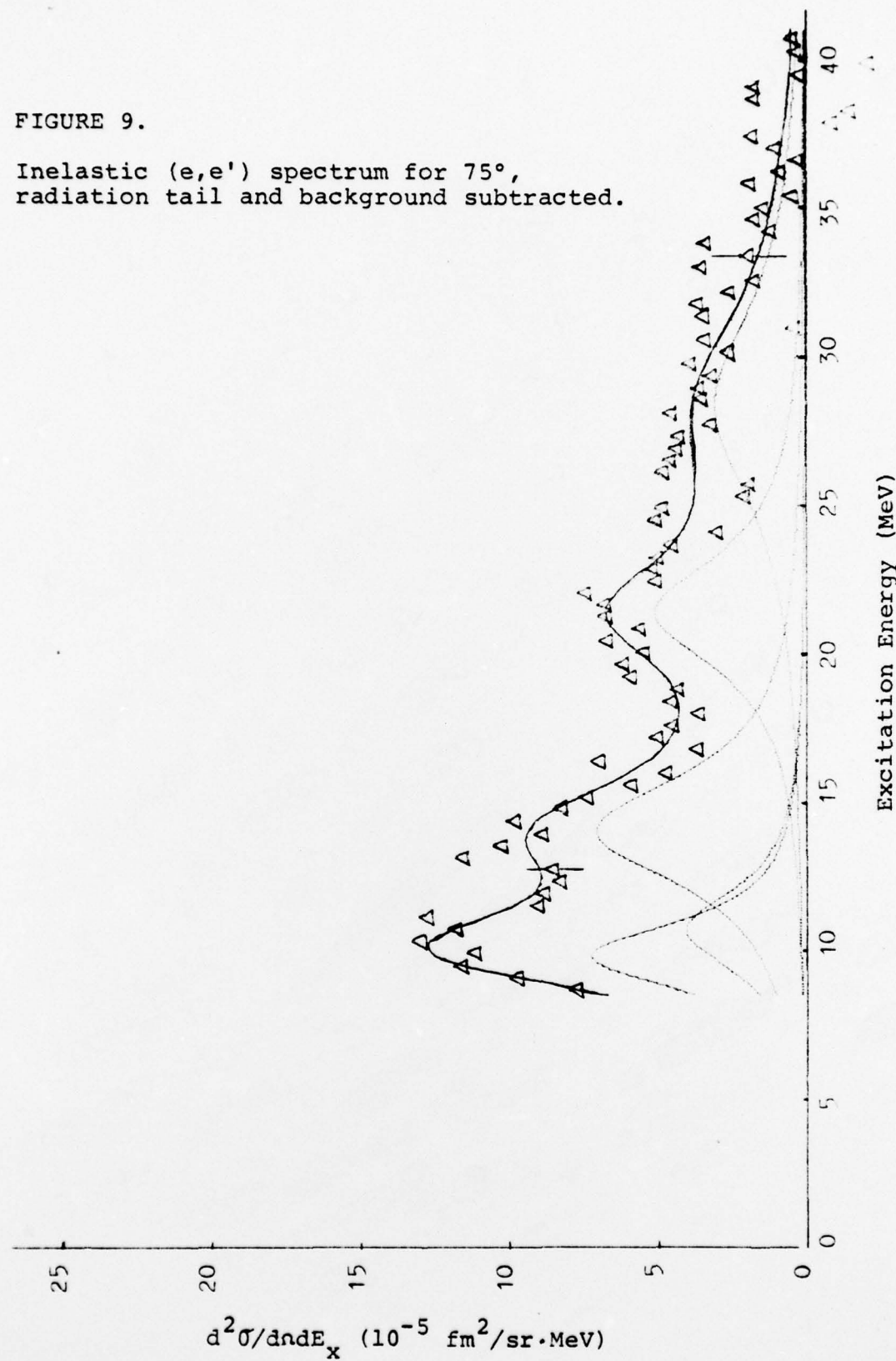
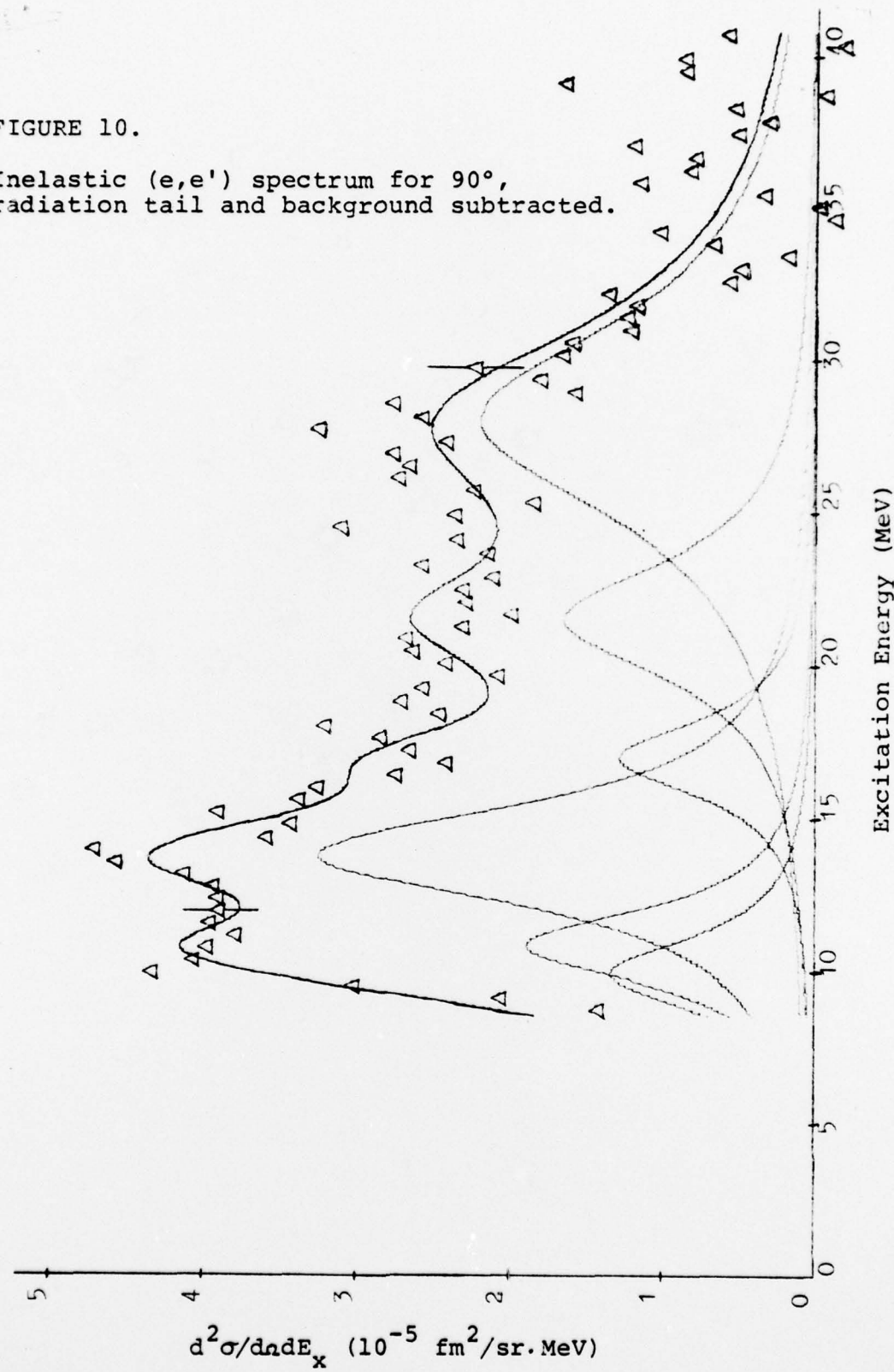


FIGURE 10.

Inelastic (e, e') spectrum for 90° ,
radiation tail and background subtracted.



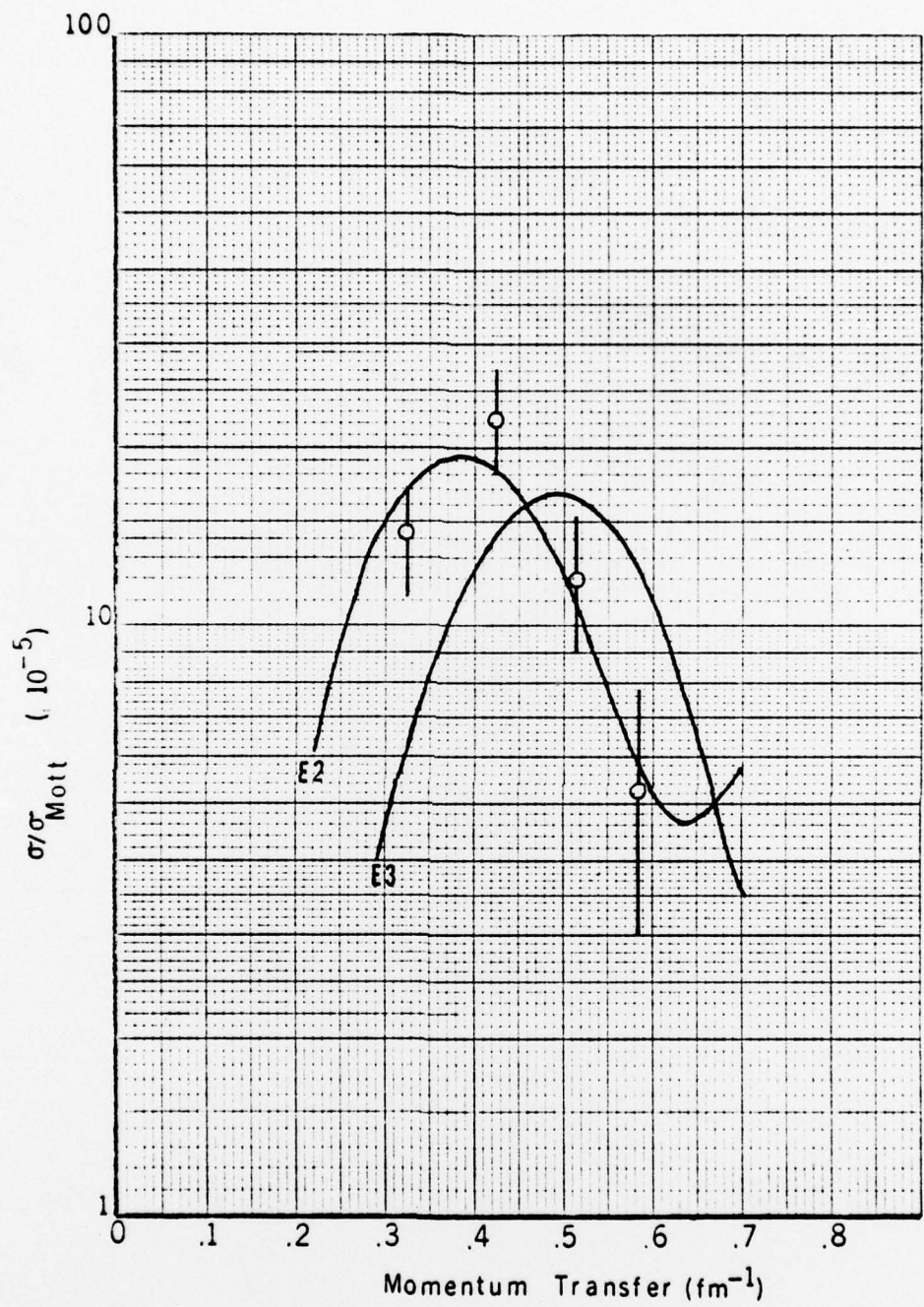


FIGURE 11.

Inelastic cross section for E2 resonance at 9.88 MeV.

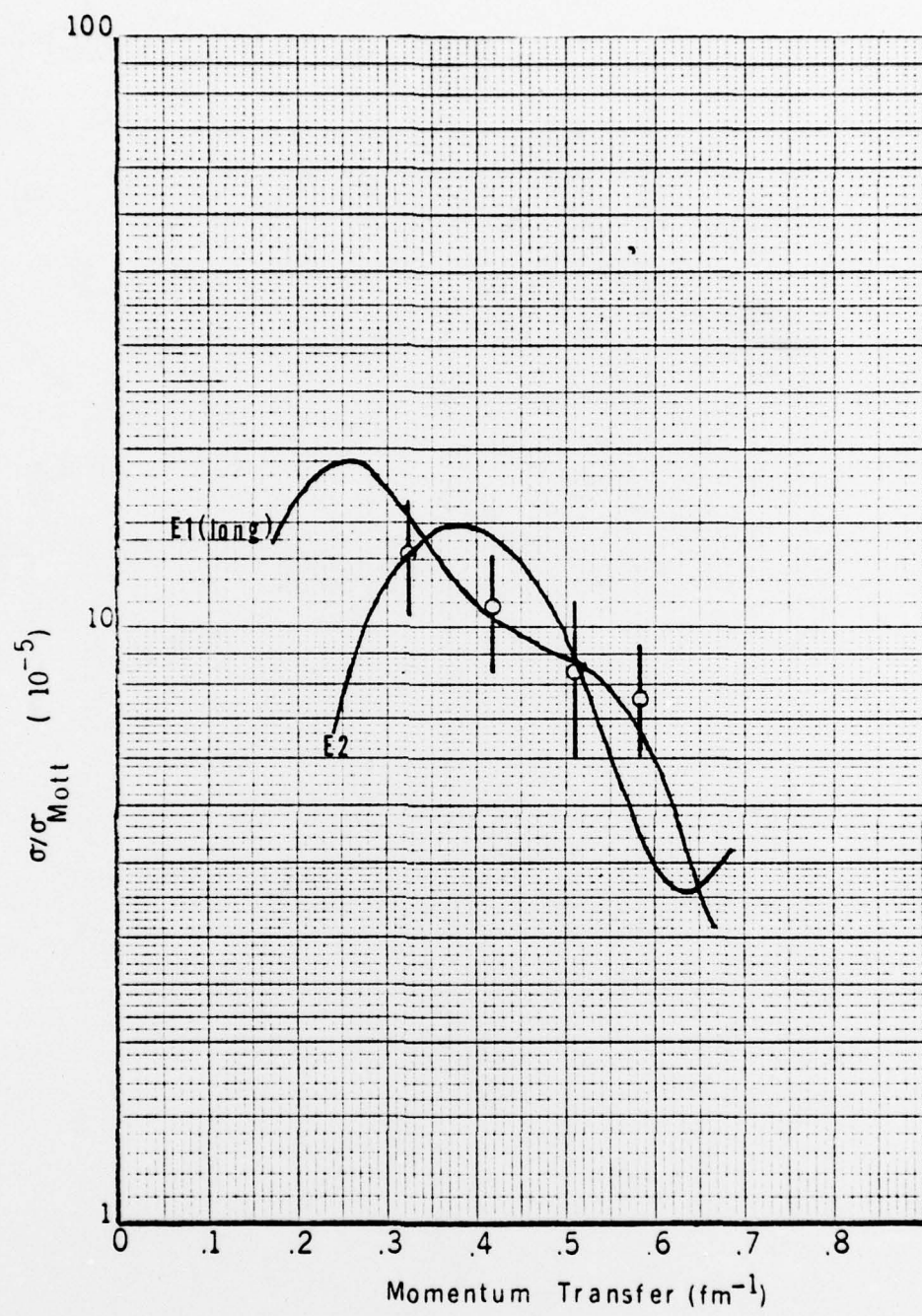


FIGURE 12.

Inelastic cross section for $E1$ (long axis) resonance at 10.77 MeV.

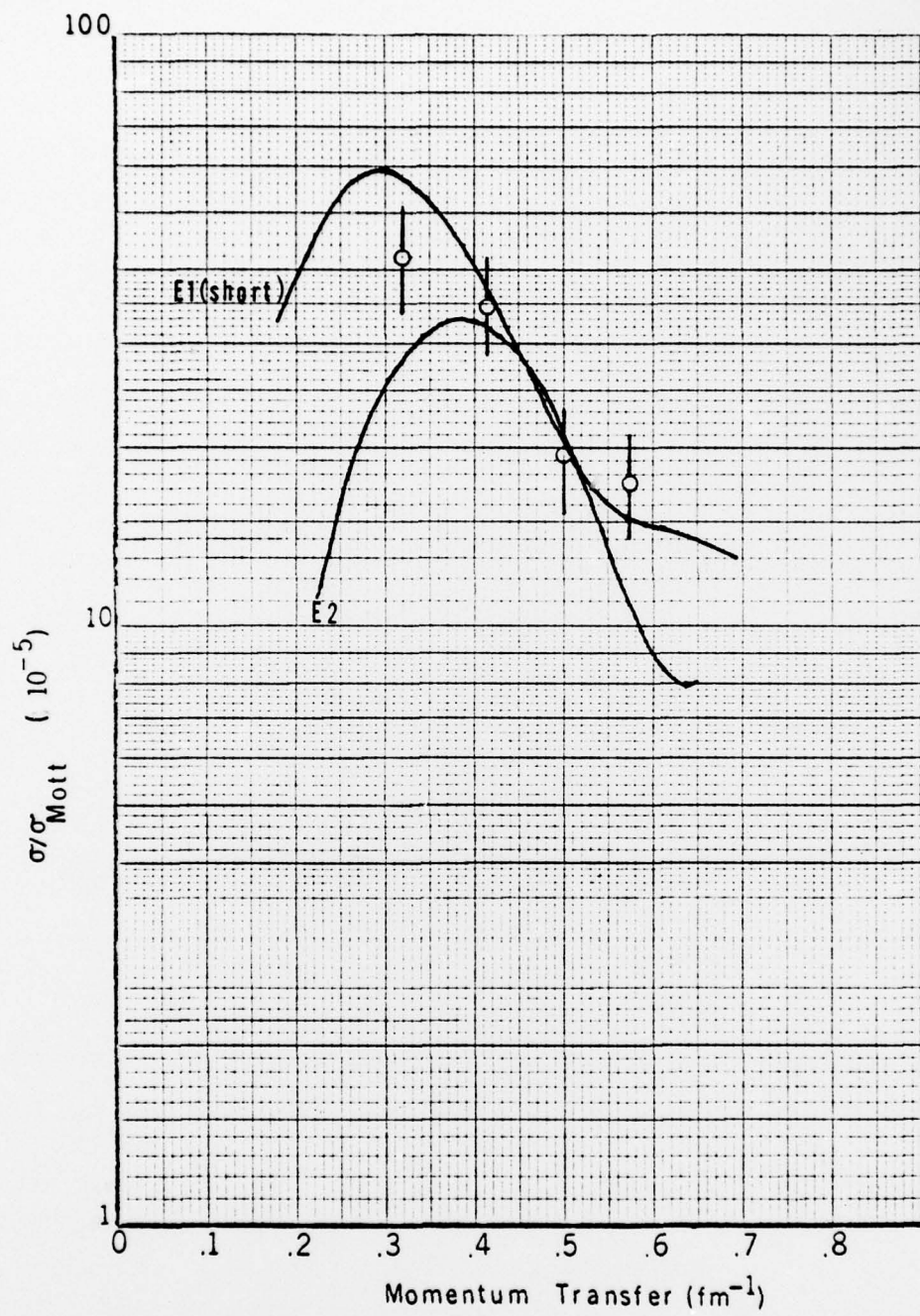


FIGURE 13.

Inelastic cross section for $E1$ (short axis) resonance at 13.94 MeV.

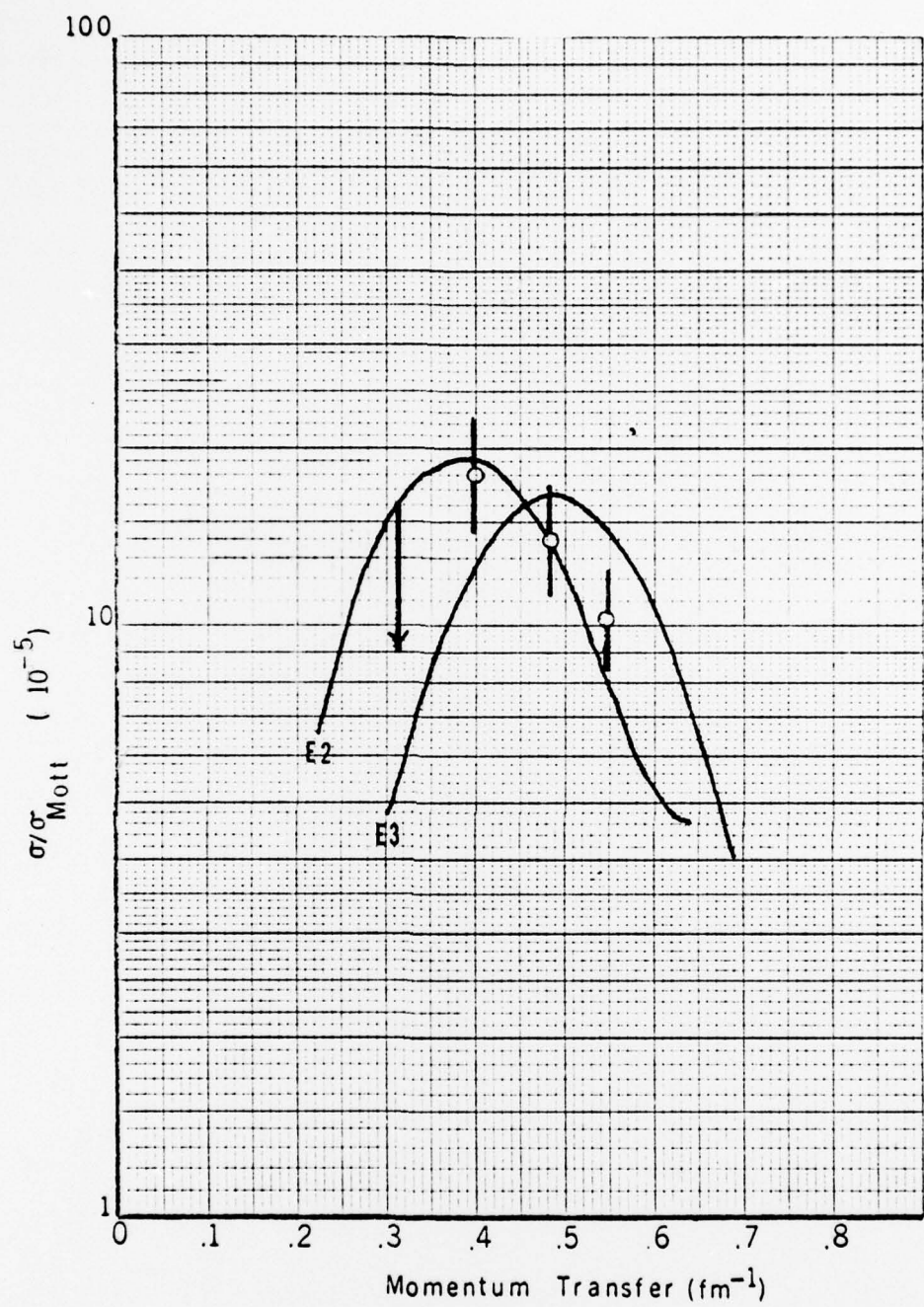


FIGURE 14.

Inelastic cross section for E2 resonance at 21.55 MeV.

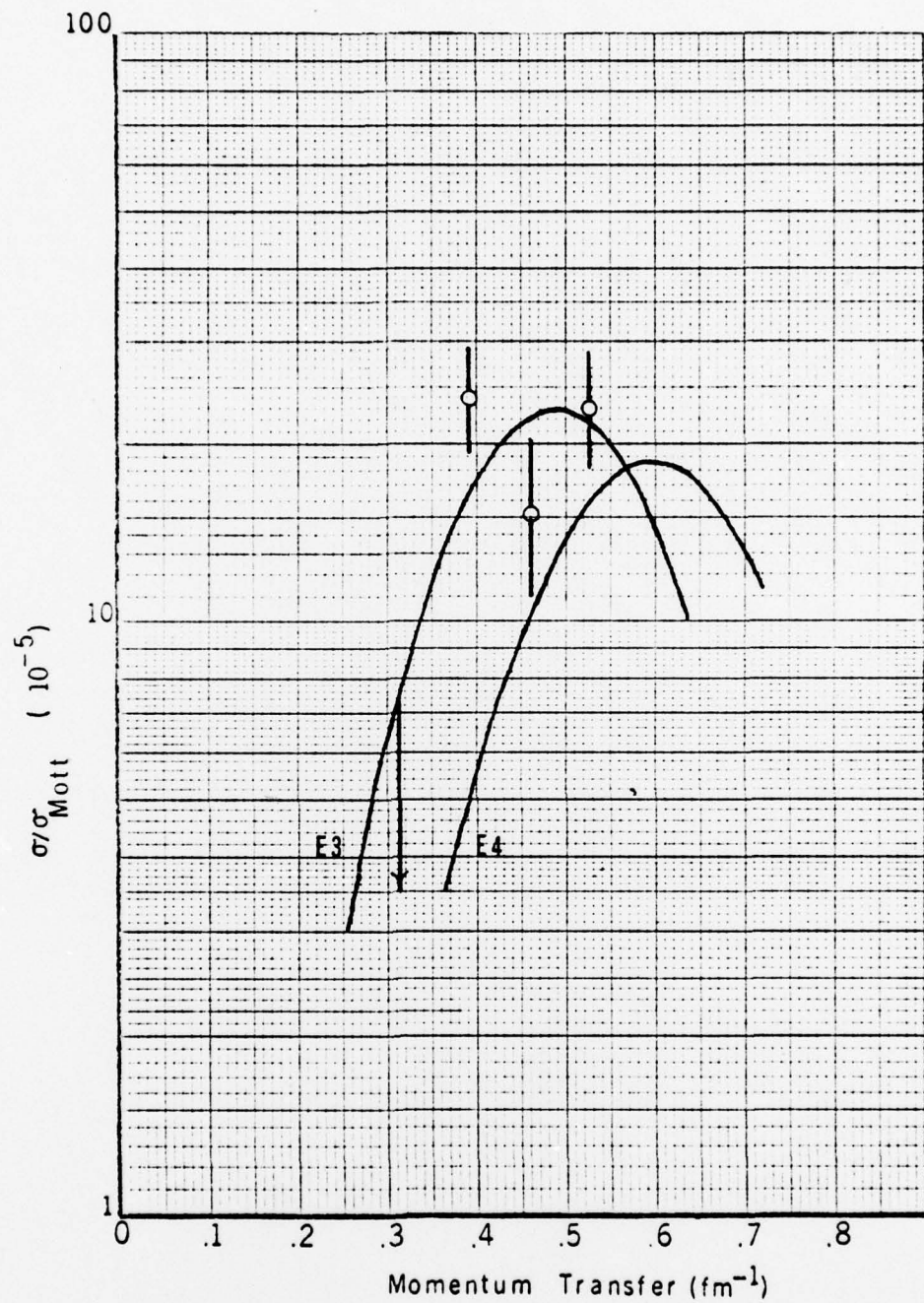


FIGURE 15.

Inelastic cross section for E3 resonance at 28.40 MeV.

FIGURE CAPTIONS

- Figure 1. DWBA cross sections for E1 to E4 transitions divided by the Mott cross section. The cross sections are based on the Goldhaber-Teller model for a spherical nucleus with the c, t values from Ref. (DeJD 74). All curves are normalized to equalize the first maxima.
- Figure 2. DWBA cross sections for the E1 transitions associated with the long and short axes of the ^{238}U prolate spheroid.
- Figure 3. Spectrum of 87.5 MeV electrons scattered inelastically from ^{238}U under 45° . Background and radiation tail are included and the count rate has been corrected for the constant momentum dispersion of the magnetic spectrometer. Note the suppressed vertical scale.
- Figure 4. Same as Figure 3 but for 60° .
- Figure 5. Same as Figure 3 but for 75° .
- Figure 6. Same as Figure 3 but for 90° .
- Figure 7. Spectrum of 87.5 MeV electrons scattered inelastically from ^{238}U under 45° . The fitted background (consisting of radiation tail caused by photon emission, general room background and the background consisting of electrons originally scattered by the target but additionally scattered by the walls of the spectrometer) has been subtracted showing clearly the relative peak heights of the various resonances. The count rate has been corrected for the constant momentum dispersion of the magnetic spectrometer. Comparison of the resonances in Figures 7 through 10 indicate the various multipolarities. The ghost peak ($E_x = 6.2$ MeV, $\Gamma = 4.5$ MeV) has been subtracted from this spectrum. The error raises with excitation energy due to the correction for the constant momentum dispersion of the magnetic spectrometer.
- Figure 8. Same as Figure 7 but for 60° .
- Figure 9. Same as Figure 7 but for 75° .
- Figure 10. Same as Figure 7 but for 90° .

Figure 11. Comparison of relative DWBA and experimental cross sections for the resonance found at 9.9 MeV. This nicely fits the E2 DWBA cross section but is definitely not an E3 resonance. 39% of the isoscalar E2 EWSR is exhausted.

Figure 12. Relative DWBA cross section for GDR long axis ($E_x = 10.8$ MeV) is plotted as reported by Gurevich, et. al. (GurL 76). The experimental E1 results of this work fit exactly to the photonuclear data. Also included for comparison is the E2 DWBA cross section.

Figure 13. Same as Figure 12 but for E1 short axis ($E_x = 13.9$ MeV). Results of this work do not fit the photonuclear data as well as the GDR long axis, but they are very close. The point at momentum transfer of $.32 \text{ fm}^{-1}$ (45°) is being affected by the ghost peak more than any of the others.

Figure 14. Relative DWBA cross sections using the Goldhaber-Teller model as compared to the resonance at 21.6 MeV with $\Gamma = 5.0$ MeV. The point indicating 45° information ($.31 \text{ fm}^{-1}$) is an upper limit to what the curve fitting program would accept with $\chi^2 < 1$. Favoring an E2 configuration over an E3, it exhausts 50% of the isovector E2 EWSR.

Figure 15. Relative DWBA cross section using the Goldhaber-Teller model for the structure at 28.4 MeV with a width of 8.1 MeV. Once again, 45° ($.31 \text{ fm}^{-1}$) is an upper limit to what would fit into the spectrum. An E3 assignment is favored over E4 and 88% of the isovector E3 EWSR is exhausted.

LIST OF REFERENCES

- BarM 74 Bar-noy, T. and Moreh, R.: Nucl. Phys., A229, 417, 1974.
- BerB 68 Bergère, R., Beil, H., Veyssièrè, A.: Nucl. Phys., A121, 463, 1968
- BerK 69 Berman, B. L., Kelly, M. A., Bramblett, R. L., Caldwell, J. T., Davis, H. S., Fultz, S. C.: Phys. Rev., 185, 1576, 1969.
- BohM 75 Bohr, A. and Mottelson, B. R.: Nuclear Structure, V. 2, W. A. Benjamin Inc., Reading, Massachusetts, 1975.
- CalD 76 Caldwell, J. T., Dowdy, E. J., Berman, B. L., Alvarez, R. A., Meyer, P.: Los Alamos Scientific Laboratory Report LA-UR76-1615, quoted in Lawrence Livermore Laboratory Report UCRL-78482, Atlas of Photoneutron Cross Sections Obtained with Monoenergetic Photons, by B. L. Berman, 30 December 1976.
- Dan 58 Danos, M.: Nucl. Phys., 5, 23, 1958.
- DeJD 74 DeJager, C. W., DeVries, H., DeVries, C.: Atomic Data and Nuclear Data Tables, 14, 479, 1974.
- FisR 64 Fischer, C. R., and Rawitscher, G. H.: Phys. Rev., 135, B377, 1964.
- GinP 64 Ginsberg, E. S. and Pratt, R. H.: Phys. Rev., 134, 4, B773, 1964.
- Goldhaber, M. and Teller, E.: Phys. Rev., 74, 1046, 1948.
- Gor 75 Gordon, E. F.: M. S. Thesis, Naval Postgraduate School, December 1975 (Unpublished).
- GurL 76 Gurevich, G. M., Lazareva, L. E., Mazur, V. M., Solodukhov, G. V. and Tulupov, B. A.: Nucl. Phys., A273, 326, 1976.
- Ham 72 Hamamoto, I.: in Proc. of the Int. Conf. on Nuclear Structure Studies Using Electron Scattering and Photoreaction, ed. by K. Shoda and H. Uji, Suppl. Res. Rep. Lab. of Nucl. Sci., Tohoku Univ., V. 5, 1972.

- Irv 72 Irvine, J. M.: Nuclear Structure Theory, Pergamon Press, Elmsford, New York, 300, 1972.
- LewH 74 Lewis, M. B., and Horen, D. J.: Phys. Rev., C10, 1099, 1974.
- Mig 44 Migdal, A.: J. Phys. USSR, 8, 331, 1944.
- MooB 76 Moore, G. L., Buskirk, F. R., Dally, E. B., Dyer, J. N., Maruyama, X. K. and Pitthan, R.: Z. Naturforsch, 31a, 668, 1976.
- NatN 66 Nathan, O. and Nilsson, S. G.: Alpha-, Beta- and Gamma-Ray Spectroscopy, ed. by Kai Siegbahn, North-Holland Publishing Company, Amsterdam, p. 601, 1966.
- PitB 74 Pitthan, R., Buskirk, F. R., Dally, E. B., Dyer, J. N., and Maruyama, X. K.: Phys. Rev. Letters, 33, 849, 1974.
- PitB 77 Pitthan, R., Buskirk, F. R., Dally, E. B., Shannon, J. O. and Smith, W. H.: (to be published).
- PitW 71 Pitthan, R. and Walcher, T.: Phys. Letters, 36B, 563, 1971.
- Sat 74 Satchler, G. R.: Phys. Rep., 14, 97, 1974.
- SteJ 50 Steinwedel, H. and Jensen J. H. D.: Z. Naturforsch, 5a, 413, 1950.
- Szy 70 Szymanski, Z.: Theory of Nuclear Structure, Trieste Lectures 1969, IAEA, Vienna, 1970
- The 72 Theissen, H.: Springer Tracts in Modern Physics Vol 65, Springer-Verlag, Berlin, 1972.
- TuaW 68 Tuan, S. T., Wright, L. E., Onley, D. S.: Nucl. Instr. Meth., 60, 70, 1968.
- Ube 71 Überall, H.: Electron Scattering from Complex Nuclei, V. 2, Academic Press, 1971.
- VeyB 73 Veyssi  re, A., Beil, H., Berg  re, R., Carlos, P., Lepr  tre, A. and Kernbath, K.: Nucl. Phys., A199, 45, 1973.
- WarW 69 Warburton, E. K. and Wenner, J.: The Role of Isospin in Electromagnetic Transitions, ed. by Wilkinson, D. H., North-Holland Publishing Company, Amsterdam, 1969.

WolM 76 Wolyne, E., Martins, M. N. and Moscati, G.: Phys.
Rev. Letters, 37, 585, 1976.

ZieP 68 Ziegler, J. F. and Peterson, G. A.: Phys. Rev.,
165, 1337, 1968.

INITIAL DISTRIBUTION LIST

	No. Copies
1. Defense Documentation Center Cameron Station Alexandria, Virginia 22314	2
2. Library, Code 0142 Naval Postgraduate School Monterey, California 93940	2
3. Physics Library, Code 61 Department of Physics and Chemistry Naval Postgraduate School Monterey, California 93940	2
4. Professor F. R. Buskirk, Code 61Bs Department of Physics and Chemistry Naval Postgraduate School Monterey, California 93940	5
5. Professor R. Pitthan, Code 61Pt Department of Physics and Chemistry Naval Postgraduate School Monterey, California 93940	5
6. Professor J. N. Dyer, Code 61Dy Department of Physics and Chemistry Naval Postgraduate School Monterey, California 93940	1
7. LCDR R. W. Moore, SMC 1541 Naval Postgraduate School Monterey, California 93940	1
8. LT W. A. Houk, SMC 1826 Naval Postgraduate School Monterey, California 93940	1